

Hydrophilic-to-Hydrophobic Volume Ratios as Structural Determinant in Small-Length Scale Amphiphilic Crystalline Systems: Silver Salts of Phenylacetylene Nitriles with Pendant Oligo(ethylene Oxide) Chains

Zhengtao Xu, Y.-H. Kiang, Stephen Lee,* Emil B. Lobkovsky, and Nathan Emmott

Contribution from the Department of Chemistry and Chemical Biology, Baker Laboratory, Cornell University, Ithaca, New York 14853-1301

Received February 23, 2000. Revised Manuscript Received May 20, 2000

Abstract: A series of 13 silver salts of phenylacetylene nitriles with pendant oligo(ethylene oxide) side chains have been crystallized, and their structures have been determined by single-crystal X-ray methods. All the organic molecules are amphiphilic in that they contain either a hydrophobic rigid linear or 3-fold planar phenylacetylene backbone to which are attached four to six rather plastic hydrophilic oligo(ethylene oxide) side chains. Six of the crystal structures have one-dimensional coordination networks based on Ag–N and Ag–O bonding, while the remainder are two-dimensional. Considering the hydrophilic and hydrophobic portions of these crystals as separate components of the crystal structure, five of the crystal structures contain parallel columns of hydrophobic moieties within a matrix of hydrophilic groups, four contain layers of hydrophilic and hydrophobic portions stacked one on top of the other, two have perforated lamellar structures and two are bicontinuous. Volume ratios of hydrophilic to hydrophobic portions prove a strong determinant as to which crystal topology is adopted for a given crystal composition. Such volume ratios can be calculated from knowledge of the molecular structure alone. A comparison is made to similar columnar and lamellar structures found in block copolymers and liquid crystalline systems. Finally, a similar breakdown of crystal topology as a function of volume ratios is found for aromatic-oligo(ethylene oxide) molecules in the Cambridge Structural Database.

Introduction

There has recently been a renewed interest in coordination and hydrogen bonded organic extended solids.^{1–42} This effort has in part been driven by the physical properties of such

materials, which include porosity^{43–62} potentially useful in separation and catalysis, magnetism,^{63–67} electronic^{33,68–70} and optical properties,⁷¹ and even moderately high T_c superconduc-

* Author to whom correspondence should be addressed.

- (1) Simard, M.; Su, D.; Wuest, J. D. *J. Am. Chem. Soc.* **1991**, *113*, 4696.
- (2) Abrahams, B. F.; Hoskins, B. F.; Lin, J.; Robson, R. *J. Am. Chem. Soc.* **1991**, *113*, 3045.
- (3) Ermer, O.; Lindenberg, L. *Helv. Chim. Acta* **1991**, *74*, 825.
- (4) Ung, A.; Gizachew, D.; Bishop, R.; Scudder, M.; Dance, I.; Craig, D. *J. Am. Chem. Soc.* **1995**, *117*, 8475.
- (5) Lu, J.; Harrison, W. T. A.; Jacobson, A. J. *Angew. Chem., Int. Ed. Engl.* **1995**, *34*, 2557.
- (6) Endo, K.; Sawaki, T.; Koyanagi, M.; Kobayashi, K.; Masuda, H.; Aoyama, Y. *J. Am. Chem. Soc.* **1995**, *117*, 8341.
- (7) Dolbecq, A.; Boubekour, K.; Batail, P.; Canadell, E.; Aubansenzier, P.; Coulon, C.; Lerstrup, K. *Mater. Chem.* **1995**, *5*, 1707.
- (8) Carlucci, L.; Ciani, G.; Proserpio, D.; Sironi, A. *Chem. Commun.* **1996**, 1393.
- (9) Vaid, T. P.; Lobkovsky, E. B.; Wolczanski, P. T. *J. Am. Chem. Soc.* **1997**, *119*, 8742.
- (10) MacGillivray, L.; Atwood, J. *Nature (London)* **1997**, *389*, 496.
- (11) Aakeröy, C. B.; Beatty, A. M.; Leinen, D. S. *J. Am. Chem. Soc.* **1998**, *120*, 7383.
- (12) Kobayashi, K.; Koyanagi, M.; Endo, K.; Masuda, H.; Aoyama, Y. *Chem. Eur. J.* **1998**, *4*, 417.
- (13) Bailey, R. D.; Hook, L. L.; Pennington, W. T. *Chem. Commun.* **1998**, 1181.
- (14) Batten, S. R.; Robson, R. *Angew. Chem., Int. Ed.* **1998**, *37*, 1461.
- (15) Hagrman, P. J.; Hagrman, D.; Zubieta, J. *Angew. Chem., Int. Ed.* **1999**, *38*, 2639.
- (16) Hagrman, D.; Hagrman, P. J.; Zubieta, J. *Angew. Chem., Int. Ed.* **1999**, *38*, 3165.
- (17) Hagrman, P. J.; Zubieta, J. *Inorg. Chem.* **1999**, *38*, 4480.
- (18) Prince, R. B.; Okada, T.; Moore, J. S. *Angew. Chem., Int. Ed.* **1999**, *38*, 233.

- (19) Gong, B.; Zheng, C.; Zeng, H. Q.; Zhu, J. *J. Am. Chem. Soc.* **1999**, *121*, 9766.
- (20) Gong, B.; Yan, Y. F.; Zeng, H. Q.; Skrzypczak-Jankun, E.; Kim, Y. W.; Zhu, J.; Ickes, H. *J. Am. Chem. Soc.* **1999**, *121*, 5607.
- (21) Li, H.; Eddaoudi, M.; Laine, A.; O'Keeffe, M.; Yaghi, O. M. *J. Am. Chem. Soc.* **1999**, *121*, 6096.
- (22) Li, H.; Eddaoudi, M.; O'Keeffe, M.; Yaghi, O. M. *Nature (London)* **1999**, *402*, 276.
- (23) Li, H.; Laine, A.; O'Keeffe, M.; Yaghi, O. M. *Science* **1999**, *283*, 1145.
- (24) Gardner, G. B.; Venkataraman, D.; Moore, J. S.; Lee, S. *Nature (London)* **1995**, *374*, 792.
- (25) Kiang, Y.-H.; Gardner, G. B.; Lee, S.; Xu, Z.; Lobkovsky, E. J. *J. Am. Chem. Soc.* **1999**, *121*, 8204.
- (26) Bernhardt, P. V. *Inorg. Chem.* **1999**, *38*, 3481.
- (27) Dong, Y. B.; Layland, R. C.; Pschirer, N. G.; Smith, M. D.; Bunz, U. H. F.; zur Loye, H. C. *Chem. Mater.* **1999**, *11*, 1413.
- (28) Tong, M. L.; Chen, X. M.; Ye, B. H.; Ji, L. N. *Angew. Chem., Int. Ed.* **1999**, *38*, 2237.
- (29) Shi, Z.; Zhang, L.; Zhu, G.; Yang, G.; Hua, J.; Ding, H.; Feng, S. *Chem. Mater.* **1999**, *11*, 3565.
- (30) Hong, M.; Su, W.; Cao, R.; Zhang, W.; Lu, J. *Inorg. Chem.* **1999**, *38*, 600.
- (31) Karle, I. L.; Ranganathan, D.; Kurur, S. *J. Am. Chem. Soc.* **1999**, *121*, 7156.
- (32) Kitazawa, T. *Chem. Commun.* **1999**, 891.
- (33) Holliday, B. J.; Farrell, J. R.; Mirkin, C. A. *J. Am. Chem. Soc.* **1999**, *121*, 6316.
- (34) Munakata, M.; Wu, L. P.; Ning, G. L.; Kuroda-Sowa, T.; Maekawa, M.; Suenaga, Y.; Maeno, N. *J. Am. Chem. Soc.* **1999**, *121*, 4968.
- (35) Tzeng, B. C.; Schier, A.; Schmidbaur, H. *Inorg. Chem.* **1999**, *38*, 3978.
- (36) Stocker, F. B.; Staeva, T. P.; Rienstra, C. M.; Britton, D. *Inorg. Chem.* **1999**, *38*, 984.

tivity,^{72,73} and in part by the promise of accessing the full panoply of organic molecular synthesis in the optimization of these aforementioned properties. One of the chief impediments in this undertaking is that the actual physical properties depend to a great extent not just on the molecular shape but the crystalline packing and that it is, in general, difficult to envision exactly this crystal packing from a knowledge of the shape and stoichiometry of the molecular building blocks alone.

At the current time the most standard approach to rationalize crystal structure has been to detail non-isotropic intermolecular forces.^{74–79} This often leads to a clear picture of the optimal

(37) Klok, H. A.; Jolliffe, K. A.; Schauer, C. L.; Prins, L. J.; Spatz, J. P.; Möller, M.; Timmerman, P.; Reinhoudt, D. N. *J. Am. Chem. Soc.* **1999**, *121*, 7154.

(38) Evans, C. C.; Sukarto, L.; Ward, M. D. *J. Am. Chem. Soc.* **1999**, *121*, 320.

(39) Vaid, T. P.; Tanski, J. M.; Pette, J. M.; Lobkovsky, E. B.; Wolczanski, P. T. *Inorg. Chem.* **1999**, *38*, 3394.

(40) Wang, Q.; Wu, X.; Zhang, W.; Sheng, T.; Lin, P.; Li, J. *Inorg. Chem.* **1999**, *38*, 2223.

(41) Bock, H.; Lehn, J. M.; Pauls, J.; Holl, S.; Krenzel, V. *Angew. Chem., Int. Ed.* **1999**, *38*, 952.

(42) Biradha, K.; Domasevitch, K. V.; Moulton, B.; Seward, C.; Zaworotko, M. J. *Chem. Commun.* **1999**, 1327.

(43) Fujita, M.; Kwon, Y. J.; Washizu, S.; Ogura, K. *J. Am. Chem. Soc.* **1994**, *116*, 1151.

(44) Choe, W.; Kiang, Y.-H.; Xu, Z.; Lee, S. *Chem. Mater.* **1999**, *11*, 1776.

(45) Venkataraman, D.; Gardner, G. B.; Lee, S.; Moore, J. S. *J. Am. Chem. Soc.* **1995**, *117*, 11600.

(46) Sevov, S. C. *Angew. Chem., Int. Ed. Engl.* **1996**, *35*, 2630.

(47) Lohse, D. L.; Sevov, S. C. *Angew. Chem., Int. Ed. Engl.* **1997**, *36*, 1619.

(48) Ekambaram, S.; Sevov, S. C. *Angew. Chem., Int. Ed.* **1999**, *38*, 372.

(49) Yang, G. Y.; Sevov, S. C. *J. Am. Chem. Soc.* **1999**, *121*, 8389.

(50) Holland, B. T.; Isbester, P. K.; Blanford, C. F.; Munson, E. J.; Stein, A. *J. Am. Chem. Soc.* **1997**, *119*, 6796.

(51) Fujita, M.; Aoyagi, M.; Ogura, K. *Bull. Chem. Soc. Jpn.* **1998**, *71*, 1799.

(52) Holland, B. T.; Blanford, C. F.; Stein, A. *Science* **1998**, *281*, 538.

(53) Ranford, J. D.; Vittal, J. J.; Wu, D. *Angew. Chem., Int. Ed.* **1998**, *37*, 1114.

(54) Biradha, K.; Dennis, D.; MacKinnon, V. A.; Sharma, C. V. K.; Zaworotko, M. J. *J. Am. Chem. Soc.* **1998**, *120*, 11894.

(55) Bielawski, C.; Chen, Y. S.; Zhang, P.; Prest, P. J.; Moore, J. S. *Chem. Commun.* **1998**, 1313.

(56) Aakeröy, C. B.; Beatty, A. M.; Leinen, D. S. *Angew. Chem., Int. Ed.* **1999**, *38*, 1815.

(57) MacLachlan, M. J.; Coombs, N.; Ozin, G. A. *Nature (London)* **1999**, *397*, 681.

(58) Soldatov, D. V.; Ripmeester, J. A.; Shergina, S. I.; Sokolov, I. E.; Zanina, A. S.; Gromilov, S. A.; Dyadin, Y. A. *J. Am. Chem. Soc.* **1999**, *121*, 4179.

(59) Holland, B. T.; Abrams, L.; Stein, A. *J. Am. Chem. Soc.* **1999**, *121*, 4308.

(60) Chui, S.; Lo, S.; Charmant, J.; Orpen, A. G.; Williams, I. D. *Science* **1999**, *283*, 1148.

(61) Gudbjartson, H.; Biradha, K.; Poirier, K. M.; Zaworotko, M. J. *J. Am. Chem. Soc.* **1999**, *121*, 2599.

(62) Khan, M. I.; Yohannes, E.; Powell, D. *Inorg. Chem.* **1999**, *38*, 212.

(63) Karasawa, S.; Sano, Y.; Akita, T.; Koga, N.; Itoh, T.; Iwamura, H.; Rabu, P.; Drillon, M. *J. Am. Chem. Soc.* **1998**, *120*, 10080.

(64) Kou, H. Z.; Bu, W. M.; Liao, D. Z.; Jiang, Z. H.; Yan, S. P.; Fan, Y. G.; Wang, G. L. *J. Chem. Soc., Dalton Trans.* **1998**, 4161.

(65) Kaul, B. B.; Durfee, W. S.; Yee, G. T. *J. Am. Chem. Soc.* **1999**, *121*, 6862.

(66) Heintz, R. A.; Zhao, H.; Ouyang, X.; Grandinetti, G.; Cowen, J.; Dunbar, K. R. *Inorg. Chem.* **1999**, *38*, 144.

(67) Monfort, M.; Resino, I.; Ribas, J.; Stoekli-Evans, H. *Angew. Chem., Int. Ed.* **2000**, *39*, 191.

(68) Mitzi, D. B.; Feild, C. A.; Harrison, W. T. A.; Guloy, A. M. *Nature (London)* **1994**, *369*, 467.

(69) Mitzi, D. B.; Wang, S.; Feild, C. A.; Chess, C. A.; Guloy, A. M. *Science* **1995**, *267*, 1473.

(70) Tang, Z.; Guloy, A. M. *J. Am. Chem. Soc.* **1999**, *121*, 452.

(71) Lin, W.; Wang, Z.; Ma, L. *J. Am. Chem. Soc.* **1999**, *121*, 11249.

(72) Tanigaki, K.; Ebbesen, T. W.; Saito, S.; Mizuki, J.; Tsai, J. S.; Kubo, Y.; Kuroshio, S. *Nature (London)* **1991**, *352*, 222.

(73) Rosseinsky, M. J.; Murphy, D. W.; Fleming, R. M.; Zhou, O. *Nature (London)* **1993**, *364*, 425.

local packing environment around any given molecule from which one may at times infer suggestions as to the global crystal structure. For example, Robson and others^{80–84} have found that there is often a strong analogy between the extended networks adopted by organic extended solids and common inorganic crystal structure types. The development of further methods in correlating molecular shape to crystalline topology nevertheless remains an essential problem in the field.

By comparison, the situation for large-length scale organic systems such as block copolymers and liquid crystals is much firmer.^{85–88} Over the last several decades a clear picture of crystalline topologies has emerged. In such systems there are generally two components (e.g., hydrophilic and hydrophobic fractions) which separate on a nanometer length scale. The resultant principal structure types include the spherical, columnar, bicontinuous, perforated lamellar, and lamellar topologies where the topology is defined by the interface between the two components. Furthermore, on the basis of the volume ratio of the two components and the degree of interfacial incompatibility one can predict the evolution of the adopted crystalline topologies.

In this contribution we study the usefulness of such large-length scale interfacial concepts in the rationalization of coordination bonded extended solids. In particular, we examine these interfaces as one approaches crystalline cell axes only an order of magnitude larger than the individual atomic bonds. We have prepared 13 crystalline compounds based on rigid hydrophobic phenylacetylene nitrile cores to which nonrigid hydrophilic oligo(ethylene oxide) side chains have been covalently attached. These molecules are then joined together through coordination bonds to silver ions. We find a direct analogy between the topology of these crystal structures and those found in the block copolymer and liquid crystalline literature. Crystal types adopted are of the columnar, perforated lamellar, lamellar, and bicontinuous types. The type adopted appears to be optimal in terms of both the hydrophobic-to-hydrophilic volume ratio and the local bonding requirements of the individual molecules. A study of crystal structures found in the Cambridge Structural Database (CSD) reveals the interface structure types reported in this paper tracks closely those found in other related non-coordination bonded organic solids.

Experimental Section

General Procedure. Unless otherwise indicated, all commercially available reagents were purchased from Aldrich and used without further purification. Analytical grade solvents were obtained from commercial suppliers (Aldrich, Fisher Scientific and Mallinckrodt). Synthesis of

(74) Gavezzotti, A. *Acc. Chem. Res.* **1994**, *27*, 309.

(75) Gavezzotti, A. In *Structure Correlation*; Bürgi, H. B., Dunitz, J., Eds.; VCH: Weinheim, 1994; Vol. 2.

(76) Dunitz, J.; Bernstein, J. *Acc. Chem. Res.* **1995**, *28*, 193.

(77) Reddy, D. S.; Craig, D. C.; G. R. D. *J. Am. Chem. Soc.* **1996**, *118*, 4090.

(78) Dunitz, J.; Taylor, R. *Chem. Eur. J.* **1997**, *3*, 89.

(79) Braga, D.; Grepioni, F.; Desiraju, G. R. *Chem. Rev.* **1998**, *98*, 1375.

(80) Hoskins, B. F.; Robson, R. *J. Am. Chem. Soc.* **1989**, *111*.

(81) Hoskins, B. F.; Robson, R. *J. Am. Chem. Soc.* **1990**, *112*, 1546.

(82) Abrahams, B. F.; Hoskins, B. F.; Michail, D. M.; Robson, R. *Nature (London)* **1994**, *369*, 727.

(83) Zaworotko, M. J. *Chem. Soc. Rev.* **1994**, *23*, 283.

(84) Duncan, P. C. M.; Goodname, D. M. L.; Menzer, S.; Williams, D. *J. Chem. Commun.* **1996**, 2127.

(85) Wanka, G.; Hoffmann, H.; Ulbricht, W. *Macromolecules* **1994**, *27*, 4145.

(86) Khandpur, A. K.; Förster, S.; Bates, F. S.; Hamley, I. W.; Ryan, A. J.; Bras, W.; Almdal, K.; Mortensen, K. *Macromolecules* **1995**, *28*, 8796.

(87) Noolandi, J.; Shi, A. C.; Linse, P. *Macromolecules* **1996**, *29*, 5907.

(88) Borisch, K.; Diele, S.; Göring, P.; Müller, H.; Tschierske, C. *Liq. Cryst.* **1997**, *22*, 427.

THF (5 mL) was added. The reaction mixture was stirred for 15 min at room temperature, and then mixed with 5 mL of HCl (0.05 M). The mixture thus obtained was then poured into ice water, extracted with ether, dried over anhydrous MgSO_4 , and evaporated under reduced pressure. The residue was a reddish viscous liquid from which pure **4a** (0.24 g, 70% yield) was isolated by flash column chromatography eluted by CH_2Cl_2 and then CH_2Cl_2 /ethyl acetate (10:1): ^1H NMR (300 MHz, CDCl_3) δ 7.69 (s, 2H), 4.70 (s, 4H), 3.74–3.71 (m, 4H), 3.62–3.59 (m, 4H), 3.39 (s, 6H); ^{13}C NMR (75 MHz, CDCl_3) δ 144.4, 130.7, 128.6, 118.8, 115.2, 72.0, 70.8, 70.5, 59.4.

4-Bromo-2,6-bis-(2,5,8-trioxanonyl)-benzonitrile (4b). **4b** was synthesized in 68% yield in the same procedure as for **4a**. The eluent for column chromatography was CH_2Cl_2 /ethyl acetate (5:1): ^1H NMR (300 MHz, CDCl_3) δ 7.68 (s, 2H), 4.69 (s, 4H), 3.76–3.67 (m, 8H), 3.67–3.61 (m, 4H), 3.58–3.52 (m, 4H), 3.36 (s, 6H); ^{13}C NMR (75 MHz, CDCl_3) δ 144.5, 130.6, 128.6, 115.1, 108.4, 72.2, 70.9, 70.9, 70.8, 70.4, 59.3.

4-Bromo-2,6-bis-(2,5,8,11-tetraoxadodecyl)-benzonitrile (4c). **4c** was synthesized in 65% yield in the same procedure as **4a**. The eluent for column chromatography was CH_2Cl_2 /ethyl acetate (1:1): ^1H NMR (300 MHz, CDCl_3) δ 7.69 (s, 2H), 4.71 (s, 4H), 3.74–3.71 (m, 8H), 3.69–3.63 (m, 12H), 3.57–3.52 (m, 4H), 3.36 (s, 6H); ^{13}C NMR (75 MHz, CDCl_3) δ 144.5, 130.6, 128.6, 115.1, 108.4, 72.2, 71.0, 70.9, 70.8, 70.7, 70.4, 59.3.

1,3,5-Tris{[4-cyano-3,5-bis(2-methoxy-ethoxymethyl)phenyl]ethynyl}benzene (5a). A Schlenk tube was charged with **4a** (0.28 g, 0.77 mmol), 1,3,5-triethynylbenzene (34 mg, 0.23 mmol), triphenylphosphine (9 mg, 0.034 mmol), bis(triphenylphosphine)palladium(II) chloride (4.5 mg, 6.4×10^{-3} mmol), copper(I) iodide (2 mg, 0.01 mmol), and triethylamine (8 mL). The tube was carefully evacuated by a vacuum manifold until the solution started boiling and then back-filled with nitrogen. After being thus purged five times, the tube was sealed with a plug and stirred at 80 °C for 12 h. The reaction mixture was cooled to room temperature, poured into water, and extracted with CH_2Cl_2 (2H 10 mL). The combined organic layer was dried over anhydrous MgSO_4 , filtered, and evaporated down to a viscous liquid. Purification by flash column chromatography using a 4:1 CH_2Cl_2 /ethyl acetate mixture afforded **5a** (0.18 g, 80% yield) as a yellowish solid: ^1H NMR (300 MHz, CDCl_3) δ 7.68 (s, 9H), 4.75 (s, 12H), 3.82–3.73 (m, 12H), 3.68–3.60 (m, 12H), 3.42 (s, 18H); ^1H NMR (300 MHz, acetone- d_6) δ 7.88 (s, 3H), 7.78 (s, 6H), 4.76 (s, 12H), 3.78–3.74 (m, 12H), 3.61–3.58 (m, 12H), 3.33 (s, 18H); ^{13}C NMR (75 MHz, CDCl_3) δ 142.9, 135.2, 130.6, 127.6, 123.8, 115.4, 109.9, 91.4, 89.9, 72.0, 70.8, 70.8, 59.4; HRMS (FAB, NBA) m/z 982.4497 [$(M + 1)^+$]; calcd for $\text{C}_{57}\text{H}_{64}\text{N}_3\text{O}_{12}$, 982.4490.

1,3,5-Tris{[4-cyano-bis-(2,5,8-trioxanonyl)phenyl]ethynyl}benzene (5b). **5b** was synthesized in 92% yield with the same procedure as **5a**. Flash column chromatography using ethyl acetate followed by a 10:1 ethyl acetate/ethanol mixture furnished **5b** as a yellowish solid: ^1H NMR (300 MHz, CDCl_3) δ 7.69 (s, 3H), 7.65 (s, 6H), 4.75 (s, 12H), 3.78–3.72 (m, 24H), 3.68–3.65 (m, 12H), 3.57–3.54 (m, 12H), 3.33 (s, 18H); ^{13}C NMR (75 MHz, CDCl_3) δ 143.0, 135.1, 130.5, 127.5, 123.8, 115.4, 109.8, 91.3, 89.9, 72.2, 70.9, 70.8, 70.8, 59.4; HRMS (ESMS, Methanol) m/z 1263.63281 [$(M + \text{NH}_4)^+$]; calcd for $\text{C}_{69}\text{H}_{91}\text{N}_4\text{O}_{18}$, 1263.63284.

1,3,5-Tris{[4-cyano-3,5-bis(2,5,8,11-tetraoxadodecyl)phenyl]ethynyl}benzene (5c). **5c** was synthesized in 85% yield with the same procedure as for **5a**. Flash column chromatography using ethyl acetate followed by a 10:1 ethyl acetate/ethanol mixture afforded **5c** as a yellowish viscous liquid: ^1H NMR (300 MHz, CDCl_3) δ 7.69 (s, 3H), 7.65 (s, 6H), 4.75 (s, 12H), 3.80–3.72 (m, 24H), 3.70–3.66 (m, 24H), 3.66–3.61 (m, 12H), 3.55–3.50 (m, 12H), 3.33 (s, 18H). ^{13}C NMR (75 MHz, CDCl_3) δ 143.0, 135.0, 130.3, 127.4, 123.8, 115.2, 109.8, 91.2, 89.9, 72.8, 72.7, 71.5, 71.4, 70.9, 70.8, 70.2, 58.7; HRMS (FAB, NBA) m/z 1510.7656 [$(M + 1)^+$]; calcd for $\text{C}_{81}\text{H}_{112}\text{N}_3\text{O}_{24}$, 1510.7636].

4,4'-Dicyano-3,3',5,5'-tetrakis-(2-methoxy-ethoxymethyl)-biphenyl (6a). A Schlenk flask was charged with bis(pinacolato) diborane (0.219 g, 0.863 mmol), **4a** (0.284 g, 0.785 mmol), tetrakis(triphenylphosphine)palladium (28 mg, 0.024 mmol), potassium acetate (0.23 g, 2.32 mmol), and DMSO (5 mL). The flask was degassed, back-filled with nitrogen, and then heated to 80–85 °C for 2 h. The reaction

mixture was then cooled to room temperature, poured into ice-water, and extracted with ether (2H 15 mL). The organic phase was dried over anhydrous MgSO_4 , filtered, and evaporated down to a viscous residue. Flash column chromatography eluted by a 30:1 CH_2Cl_2 /THF mixture afforded **6a** (0.12 g, 55% yield) as a yellowish solid: ^1H NMR (300 MHz, CDCl_3) δ 7.77 (s, 4H), 4.80 (s, 8H), 3.81–3.73 (m, 8H), 3.68–3.59 (m, 8H), 3.40 (s, 12H); ^{13}C NMR (75 MHz, CDCl_3) δ 143.9, 143.4, 126.7, 115.6, 110.4, 72.0, 71.1, 70.8, 59.4; HRMS (FAB, NBA) m/z 557.2866 [$(M + 1)^+$]; calcd for $\text{C}_{30}\text{H}_{41}\text{N}_3\text{O}_8$, 557.2863].

4,4'-Dicyano-3,3',5,5'-tetrakis-(2,5,8-trioxanonyl)-biphenyl (6b). **6b** was synthesized in 45% yield with the same procedure as for **6a**. Column chromatography eluted by 5:1 CH_2Cl_2 /THF and then 3:1 CH_2Cl_2 /THF afforded the product as a slightly yellow, viscous liquid: ^1H NMR (300 MHz, CDCl_3) δ 7.72 (s, 4H), 4.80 (s, 8H), 3.83–3.76 (m, 8H), 3.76–3.70 (m, 8H), 3.69–3.62 (m, 8H), 3.57–3.50 (m, 8H), 3.34 (s, 12H); ^{13}C NMR (75 MHz, CDCl_3) δ 144.0, 143.5, 126.8, 115.6, 110.4, 72.2, 71.1, 70.9, 70.8, 59.3. ESMS (methanol) m/z 755.5 ($M + \text{Na}$) $^+$.

2,6-Bis-(2-methoxy-ethoxymethyl)-4-trimethylsilyl-benzonitrile (7a). A heavy-walled Schlenk tube equipped with a magnetic stirrer was charged with (**4a**) (0.95 g, 2.6 mmol), copper(I) iodide (5 mg, 0.026 mmol), bis(triphenylphosphine)palladium(II) chloride (29.9 mg, 0.052 mmol), triphenylphosphine (68 mg, 0.26 mmol), and triethylamine (10 mL). The tube was carefully evacuated by a vacuum manifold until the solution started boiling and then back-filled with nitrogen. After being thus purged 5 times, trimethylsilylacetylene (0.80 mL, 5.6 mmol), previously stored under nitrogen, was added to the flask under nitrogen via syringe. The tube was then sealed with a septum and stirred at 70 °C for 15 h. The reaction mixture was then allowed to cool to room temperature and was filtered through a fritted glass funnel. The filtrate was evaporated to dryness under reduced pressure on a rotary evaporator on silica gel (9:1 CH_2Cl_2 :ethyl acetate) to yield **7a** as a waxy solid (0.63 g, 62%): ^1H NMR (300 MHz, CDCl_3) δ 7.60 (s, 2H), 4.70 (s, 4H), 3.75–3.72 (m, 4H), 3.64–3.62 (m, 4H), 3.41 (s, 6H) 0.26 (s, 9H); ^{13}C NMR (75 MHz, CDCl_3) δ 142.3, 130.6, 127.9, 115.2, 109.4, 103.3, 99.2, 71.7, 70.6, 70.4, 59.0, –0.28.

4-Trimethylsilyl-2,6-bis-(2,5,8-trioxanonyl)-benzonitrile (7b). **7b** was synthesized with the same procedure as that for **7a** in the amount of 0.74 g (80% yield). Flash column chromatography eluted by a 5:1 CH_2Cl_2 /ethyl acetate mixture yielded **7b** as a viscous liquid: ^1H NMR (300 MHz, CDCl_3) δ 7.54 (s, 2H), 4.67 (s, 4H), 3.71–3.68 (m, 8H), 3.65–3.62 (m, 4H), 3.55–3.52 (4H, m), 3.35 (s, 6H) 0.22 (s, 9H); ^{13}C NMR (75 MHz, CDCl_3) δ 142.4, 130.5, 127.8, 115.1, 109.2, 103.3, 99.0, 71.9, 70.5, 70.4, 70.3, 59.0, –0.32.

4,4'-Dicyano-3,3',5,5'-tetrakis-(2-methoxy-ethoxymethyl)tolan (8a). **7a** (0.45 g, 1.7 mmol), potassium carbonate (0.08 g, 0.58 mmol), a methanol/dichloromethane 1:6 solution (14 mL), and a magnetic stirrer were placed in a heavy-walled Schlenk flask and stirred under nitrogen for 2 h. This mixture was transferred to another heavy-walled Schlenk flask previously charged with **7a** (0.43 g, 1.2 mmol), triphenylphosphine (31 mg, 0.12 mmol), bis(dibenzylideneacetone)palladium(0) (13 mg, 0.024 mmol), and triethylamine (4 mL). The flask was then purged with nitrogen in the same way as for **7a** and sealed with a Teflon cap. After stirring at 70 °C for 12 h, the reaction mixture was allowed to cool to room temperature and was filtered through a glass funnel. The filtrate was evaporated under reduced pressure on a rotary evaporator, and the residue was purified by column chromatography on silica gel (3:1 CH_2Cl_2 /ethyl acetate) to yield **8a** as a yellow solid (0.51 g, 73%): ^1H NMR (300 MHz, CDCl_3) δ 7.67 (s, 4H), 4.74 (s, 8H), 3.77–3.74 (m, 8H), 3.64–3.61 (m, 8H), 3.41 (s, 12H); ^{13}C NMR (75 MHz, CDCl_3) δ 142.7, 130.3, 127.1, 115.1, 109.7, 91.7, 71.8, 70.5, 59.1; HRMS (EI, 70 eV) m/z 580.2777 [M^+]; calcd for $\text{C}_{32}\text{H}_{40}\text{N}_2\text{O}_8$, 580.2785].

4,4'-Dicyano-3,3',5,5'-tetrakis-(2,5,8-trioxanonyl)tolan (8b). **8b** was synthesized with the same procedure as for **8a** in the amount of 0.52 g (47% yield). Flash column chromatography eluted by a 2:1 CH_2Cl_2 /ethyl acetate mixture yielded **8b** as a yellowish solid: ^1H NMR (300 MHz, CDCl_3) δ 7.66 (s, 4H), 4.73 (s, 8H), 3.77–3.72 (m, 16H), 3.68–3.65 (m, 8H), 3.57–3.54 (m, 8H), 3.36 (s, 12H); ^{13}C NMR (75 MHz, CDCl_3) δ 143.1, 130.6, 127.3, 118.9, 115.4, 110.0, 92.0, 72.2, 70.9, 70.8, 70.6, 59.3; HRMS (EI, 70 eV) m/z 756.3816 [M^+]; calcd for $\text{C}_{40}\text{H}_{56}\text{N}_2\text{O}_{12}$, 756.3833].

X-ray Quality Single Crystal of 8a·AgOTf (9). A solution of **8a** (5.0 mg, 8.6 μ mol) in benzene (1.5 mL) was mixed with a solution of silver triflate (2.2 mg, 8.6 μ mol) in benzene (1.5 mL). No precipitate formed immediately after mixing. Slow evaporation of the solvent over 3 days produced colorless, needlelike single crystals suitable for X-ray analysis. X-ray powder diffraction of the bulk sample (see Supporting Information) showed only one crystal phase which corresponds to the single-crystal structure.

X-ray Quality Single Crystal of 8a·AgPF₆ (10). A 500 mg benzene solution of **8a** (2.0% by weight, 0.030 M) was mixed with a 500 mg benzene solution of silver hexafluorophosphate (0.89%, 0.030 M). A white precipitate formed immediately. Enough acetone was added to dissolve all of the precipitate. Slow evaporation at room temperature over 3 weeks yielded colorless needlelike crystals suitable for X-ray analysis.

X-ray Quality Single Crystal of 8a·AgSbF₆ (11). The same method was applied as for **10**. The solutions used were a 500 mg benzene solution of **8a** (2.0%, 0.030 M) and a 500 mg benzene solution of silver hexafluoroantimonate (1.2%, 0.030 M). Colorless needles of single crystals were obtained as the final product.

X-ray Quality Single Crystal of 8b·AgSbF₆·H₂O (12). The same method was applied as for **10**. The solutions used were a solution of **8b** (10 mg, 0.013 mmol) in benzene (1.5 mL) and a solution of AgSbF₆ (4.5 mg, 0.013 mmol) in benzene (1.5 mL). Slow evaporation of the solvents over 3 days yielded colorless, needlelike single crystals suitable for X-ray analysis. X-ray powder diffraction of the bulk sample showed only one crystal phase which corresponds to the single-crystal structure.

X-ray Quality Single Crystal of 6b·4AgOTf (13). A 20 mg benzene-*d*₆ solution of **6b** (4.9%, 0.063 M), a 40 mg benzene-*d*₆ solution, and a 75 mg *m*-xylene solution of silver triflate (1.8%, 0.063 M) were sequentially placed one beneath the other in a 2 mm diameter glass tube. The tube was then sealed. Slow diffusion at ambient temperature over 1 week yielded needlelike crystals which, however, were too small for single-crystal X-ray analysis. A small cleft was cut at the tip of the tube to allow slow evaporation of the solvents for further crystallization. Colorless needles of crystals of X-ray quality were collected after another 2 weeks. X-ray powder diffraction showed only one single-crystal phase which corresponds to the pattern generated by the solved single-crystal structure.

X-ray Quality Single Crystal of 6b·2AgBF₄·H₂O (14). The same method was applied as for **10**. The solutions used were a 20 mg *m*-xylene solution of **6b** (1.3%, 0.015 M) and a 17 mg *m*-xylene solution of silver tetrafluoroborate (0.78%, 0.036 M). Blocks of colorless crystals were collected as the final product. X-ray powder diffraction showed only one single-crystal phase which corresponds to the pattern generated by the solved single-crystal structure.

X-ray Quality Single Crystal of 6b·AgBF₄·C₆H₆·H₂O (15). A 20 mg benzene-*d*₆ solution of **6b** (4.9%, 0.065 M), a 40 mg benzene-*d*₆ solution, and a 55 mg *m*-xylene solution of silver tetrafluoroborate (1.4%, 0.065 M) were sequentially placed one beneath the other in a 2 mm diameter glass tube. The tube was then sealed. Slow diffusion at ambient temperature over 1 week yielded blocks of colorless crystals suitable for X-ray analysis.

X-ray Quality Single Crystal of 6b·2AgSbF₆ (16). The same method was applied as for **10**. The solutions used were a 20 mg *m*-xylene solution of **6b** (1.3%, 0.015 M) and a 22 mg *m*-xylene solution of silver hexafluoroantimonate (1.1%, 0.028 M). Colorless needles of single crystal were obtained as the final product. X-ray powder diffraction showed only one single-crystal phase which corresponds to the pattern generated by the solved single-crystal structure.

X-ray Quality Single Crystal of 6a·2AgOTf·0.5 *m*-xylene (17). The same method was applied as for **13**. The solutions used were a 20 mg benzene-*d*₆ solution of **6a** (1.8%, 0.032 M), a 40 mg benzene-*d*₆ solution, and a 13 mg *m*-xylene solution of silver triflate (1.3%, 0.046 M). Blocks of colorless single crystals were obtained as the final product.

X-ray Quality Single Crystal of 6a·2AgBF₄ (18). The same method was applied as for **15**. The three solutions used were a 20 mg benzene-*d*₆ solution of **6a** (1.8%, 0.032 M), a 40 mg benzene-*d*₆ solution, and

a 23 mg *m*-xylene solution of silver tetrafluoroborate (1.1%, 0.05 M). Colorless needlelike single crystals were obtained as the final product. X-ray powder diffraction showed only one single-crystal phase which corresponds to the pattern generated by the solved single-crystal structure.

X-ray Quality Single Crystal of 6a·1.25AgSbF₆·1.25C₆H₆ (19). The same method was applied as for **15**. The three solutions used were a 20 mg benzene-*d*₆ solution of **6a** (1.8%, 0.032 M), a 40 mg benzene-*d*₆ solution, and a 23 mg *m*-xylene solution of silver tetrafluoroborate (1.2%, 0.031 M). Blocks of colorless single crystals were obtained as the final product. X-ray powder diffraction showed only one single-crystal phase which corresponds to the pattern generated by the solved single-crystal structure.

X-ray Quality Single Crystal of 5a·AgOTf (20). The same method was applied as for **15**. The three solutions used were a 40 mg benzene-*d*₆ solution of **5a** (1.5%, 0.015 M), a 60 mg benzene-*d*₆ solution, and a 40 mg *m*-xylene solution of silver triflate (0.4%, 0.013 M). Blocks of colorless single crystals were obtained as the final product. X-ray powder diffraction showed only one single-crystal phase which corresponds to the pattern generated by the solved single-crystal structure.

X-ray Quality Single Crystal of 5b·4AgOTf (21). The same method was applied as for **15**. The three solutions used were a 30 mg benzene-*d*₆ solution of **5b** (11%, 0.07 M), a 60 mg benzene-*d*₆ solution, and a 90 mg *m*-xylene solution of silver triflate (2.5%, 0.085 M). Blocks of colorless single crystals were obtained as the final product. X-ray powder diffraction showed only one single-crystal phase which corresponds to the pattern generated by the solved single-crystal structure.

Results

Single-Crystal Structure of 8a·AgOTf (9). The crystal structure of **9** is illustrated in Figure 1a. In this structure the silver atoms are bonded to two ligand nitrogen atoms in a nearly linear fashion at Ag–N distances of 2.12 and 2.14 Å. The silver atoms are also coordinated to one triflate counterion with a Ag–O distance of 2.44 Å. In addition, there is a rather weak Ag–Ag bond: this Ag–Ag distance of 3.23 Å is slightly shorter than twice the 1.72 Å silver van der Waal radius.⁹¹ Considering only Ag–N and Ag–O bonds, the silver atom coordination is T-shaped. It is interesting to note that although molecule **8a** contains eight oxygen atoms, none of them are coordinated to silver.

As each silver atom is bonded to two ligand nitrogen atoms and vice versa, each ligand molecule is bonded to two silver atoms, and the resulting topology contains one-dimensional (1-D) infinite chains alternating between silver atoms and ligand **8a** molecules. As one may see in Figure 1a, a unit cell contains two such 1-D infinite chains running along [1 0 -2]. Parallel chains exhibit π – π interactions at an average plane-to-plane distance 3.6 Å. Thus, considering just Ag–N and Ag–O coordination bonds the network is one-dimensional, while if π – π interactions are also included, the overall net is two-dimensional (2-D).

Single-Crystal Structure of 8a·AgPF₆ (10). The Ag atom in this structure is bonded to two **8a** molecules through Ag–N bonds 2.14 and 2.22 Å long and with an N–Ag–N angle of 145.1°. One side chain from a third **8a** molecule then chelates the Ag atom through two Ag–O bonds 2.58 and 2.50 Å long. The resultant overall coordination is sawhorse-like with the two nitrogen atoms sitting on a bent horizontal bar and the two oxygen atoms at the fulcrum.

Like **9**, the structure contains infinite chains of alternating organic molecules and Ag(I) ions, and the infinite chains stack to form a 2-D sheet (Figure 1b). The interplanar π – π distance

(91) Bondi, A. *J. Phys. Chem.* **1964**, *68*, 441.

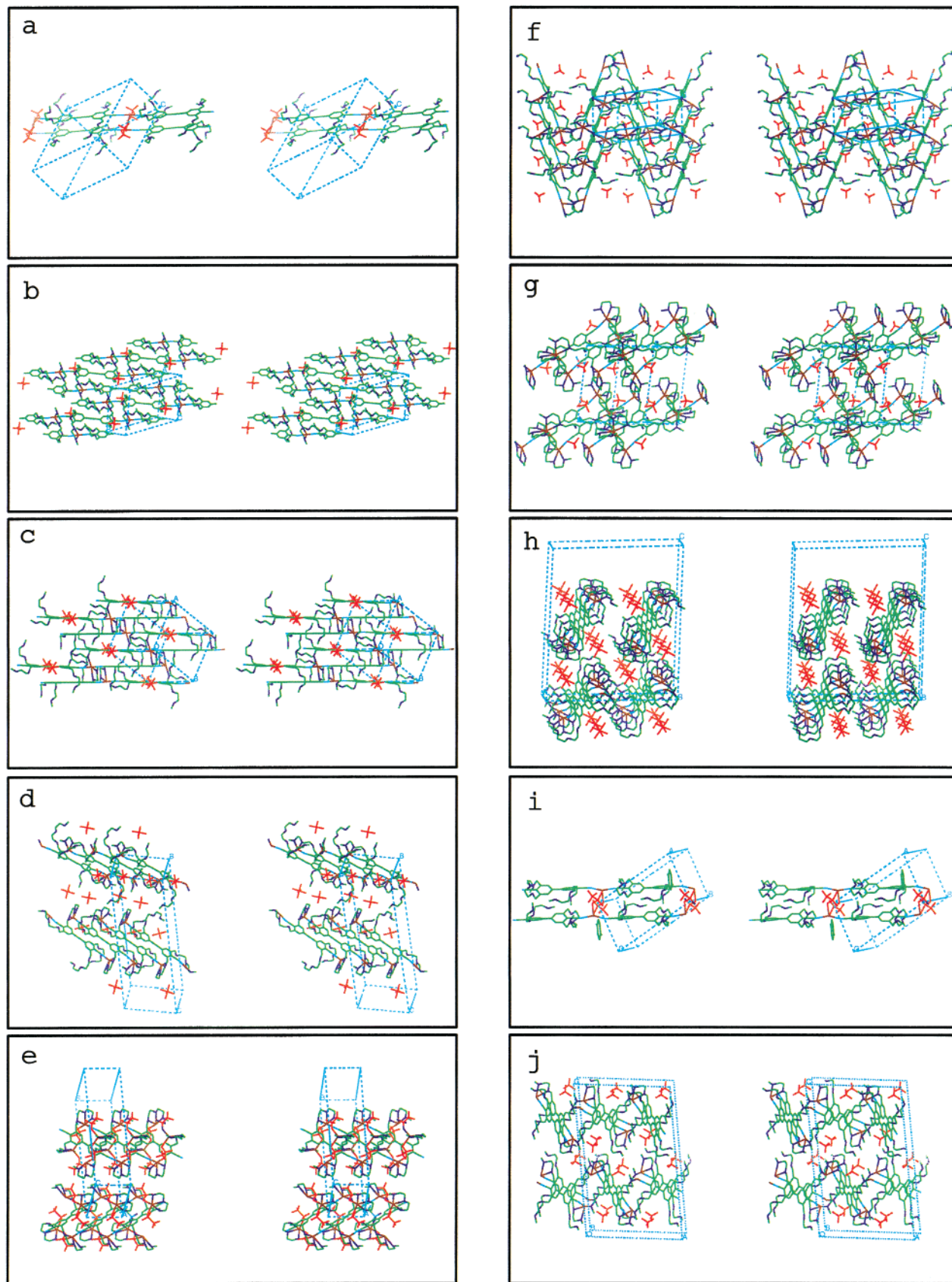


Figure 1. Stereoviews of crystal structures of (a) $8\mathbf{a}\cdot\text{AgOTf}$ (**9**), (b) $8\mathbf{a}\cdot\text{AgPF}_6$ (**10**), (c) $8\mathbf{a}\cdot\text{AgSbF}_6$ (**11**), (d) $8\mathbf{b}\cdot 2\text{AgSbF}_6\cdot 2\text{H}_2\text{O}$ (**12**), (e) $6\mathbf{b}\cdot 4\text{AgOTf}$ (**13**), (f) $6\mathbf{b}\cdot 2\text{AgBF}_4\cdot\text{H}_2\text{O}$ (**14**), (g) $6\mathbf{b}\cdot\text{AgBF}_4\cdot\text{C}_6\text{H}_6\cdot\text{H}_2\text{O}$ (**15**), (h) $6\mathbf{b}\cdot 2\text{AgSbF}_6$ (**16**), (i) $6\mathbf{a}\cdot 2\text{AgOTf}\cdot 0.5$ *m*-xylene (**17**), (j) $6\mathbf{a}\cdot 2\text{AgBF}_4$ (**18**). Counterions: red, Ag: brown, N: light blue, O: blue, C: green. For the sake of clarity, disorder in atom positions has been removed.

is roughly 3.4 Å. The overall coordination network is 2-D due to the chelation of the oxygen atoms to the Ag ions across the neighboring chains.

Single-Crystal Structure of $8\mathbf{a}\cdot\text{AgSbF}_6$ (11**).** This structure bears close resemblance to **10** in both its overall coordination topology and the way the organic molecules and the metal ions

are packed, Figure 1c. The local coordination geometry of the silver ion, however, shows some differences. While the two Ag–N bonds continue to form in a similar fashion (bond lengths, 2.179 and 2.248 Å; bond angle, 149.1°), there are three oxygen atoms coordinated to each silver atom at distances ranging from 2.48 to 2.73 Å. The overall coordination of the silver atom is a distorted trigonal bipyramid.

Single-Crystal Structure of 8b·2AgSbF₆·2H₂O (12). There are two crystallographically non-equivalent Ag atoms in the unit cell. Ag1 is coordinated to one nitrogen from a **8b** molecule, three oxygen atoms on one side chain of another **8b** molecule, and one oxygen atom from a water molecule. The hydrogen atoms of this adventitious water molecule were located through the Fourier electron density difference map. The overall coordination of Ag1 is a distorted square pyramid with an Ag–N distance of 2.25 Å and Ag–O distances ranging from 2.42 to 2.55 Å. Ag2 is coordinated to one nitrogen atom and five oxygen atoms in a distorted octahedron with an Ag–N bond length of 2.21 Å and the Ag–O distances ranging from 2.40 to 2.87 Å. The nitrogen atom and two of the oxygen atoms are derived from the same **8b** molecule, while the remaining three oxygen atoms reside on one side chain of another **8b** molecule.

As Figure 1d shows, the two nitrogen ends of each **8b** molecule are respectively capped by Ag1 and Ag2. Such Ag1–**8b**–Ag2 units then stack along the *a* axis with an interplanar distance of 3.3 Å. One of the Ag atoms of each Ag1–**8b**–Ag2 unit is bonded to a side chain from the **8b** molecule just above it in the stacking sequence, while the other is bonded to a side chain of the **8b** molecule just underneath. The resulting structure is a 1-D column of **8b** molecules and silver atoms connected through Ag–N, Ag–O bonds and π – π interactions.

Single-Crystal Structure of 6b·4AgOTf (13). There are two crystallographically non-equivalent Ag atoms in this structure. Ag1 is coordinated to one nitrogen from a **6b** molecule, three oxygen atoms on one side chain of another **6b** molecule, and one oxygen atom from a triflate ion. The overall coordination is a distorted square pyramid with an Ag–N distance of 2.184 Å and Ag–O distances ranging from 2.31 to 2.68 Å. Ag2 is coordinated to five oxygen atoms in a distorted square pyramid at distances ranging from 2.40 to 2.65 Å. Three of the oxygen atoms reside on one side chain of a **6b** molecule, while the other two are from two different triflate ions. One of the triflate ions is bonded exclusively to Ag2, and the other one has close contacts with both Ag1 and Ag2 at Ag–O distances of respectively 2.31 and 2.62 Å.

Like **12**, each organic molecule is capped by two Ag atoms, and the aromatic rings of the **6b** molecules stack in a columnar fashion along the *a* axis, Figure 1e. The interplanar π – π distance is around 3.5 Å. Again like **12**, the two Ag1 atoms on each Ag–**6b**–Ag unit are bonded to oxygen atoms from the side chain of an organic molecule lying either just above it or beneath it in the columnar sequence. The Ag–**6b**–Ag units in the column are also linked by a triflate ion. The resultant overall coordination network is one-dimensional.

Single-Crystal Structure of 6b·2AgBF₄·H₂O (14). The Ag atom in this structure is bonded to one nitrogen atom at Ag–N distance of 2.19 Å and five oxygen atoms at Ag–O distances ranging from 2.32 to 2.79 Å. The overall coordination resembles a distorted octahedron. The nitrogen atom, two of the oxygen atoms, and the other three oxygen atoms are respectively furnished by three different **6b** molecules. Also located through Fourier difference maps was an additional site near an inversion center. We assigned this site to be the oxygen of a water molecule, a suggestion supported by the fact that a possible

hydrogen atom could be located by Fourier difference maps 0.99 Å from the oxygen site.

The Ag–**6b**–Ag units stack along the *b* axis (π – π distance, 3.5 Å) to form a columnar structure. Like **12**, two of the side chains from each **6b** molecule chelate Ag atoms which lie above and below it in the columnar stack. The remaining two side chains chelate silver atoms from neighboring columns. The resultant coordination network is therefore a 2-D sheet consisting of the columns linked by these latter Ag–O bonds, as shown in Figure 1f. Disorder in the possible water molecules as well as in the BF₄ units has been removed from this drawing.

Single-Crystal Structure of 6b·3AgBF₄·C₆H₆·H₂O (15). There are three crystallographically non-equivalent Ag atoms in this structure. Ag1 is bonded in a distorted square pyramid to one nitrogen atom and four oxygen atoms. One of the oxygen atoms is from an adventitious water molecule, while the other three are derived from side chains of the **6b** molecule. The hydrogen atoms of this adventitious water molecule were also found by Fourier difference maps. The Ag1–N distance is 2.25 Å while the Ag1–O distances range from 2.39 to 2.51 Å. The Ag2 atom is bonded to one nitrogen atom and three side chain oxygen atoms at a distance range similar to that of Ag1. In addition, Ag2 weakly interacts with a benzene molecule with the closest Ag–C distance being 2.76 Å. The nitrogen atom, the oxygen atoms, and the closest carbon atom together form a distorted square pyramid around Ag2. Ag3 is coordinated to five side chain oxygen atoms in a distorted square pyramid at Ag–O distances ranging from 2.36 to 2.77 Å. The same benzene molecule that is bonded to Ag2 also interacts with Ag3, the closest Ag–C distances being 2.48 Å. Including this Ag–C interaction, Ag3 has a distorted octahedral coordination environment.

Similar to that of **12**, the coordination network of **15** is 1-D and consists of columns of Ag1–**6b**–Ag2 units stacked along the *a* axis (π – π distance, 3.5 Å), Figure 1g. Each Ag1 or Ag2 atom is chelated by side chains of **6b** molecules which are either directly above or directly beneath the Ag atom in the columnar stacking sequence. Each column is further strengthened by both the Ag3 atoms as well as the cocrystallized benzene molecule. The overall coordination network is two-dimensional.

Single-Crystal Structure of 6b·2AgSbF₆ (16). In this structure the silver atom is coordinated in a distorted square pyramid to one nitrogen atom at Ag–N distance of 2.16 Å and four oxygen atoms at Ag–O distances ranging from 2.27 to 2.60 Å. Two of the oxygen atoms and the nitrogen atom are derived from the same **6b** molecule. The other two oxygen atoms sit on one side chain of another **6b** molecule.

As seen in Figure 1h, the Ag–**6b**–Ag units stack along the *b* axis at π – π distance of 3.6 Å. Two of the side chains on each Ag–**6b**–Ag unit chelate one Ag atom from above and one from beneath, as is found in **12**–**15**. The resulting structure is a 1-D column of **6b** molecules connected through Ag–N, Ag–O bonds and π – π interactions.

Single-Crystal Structure of 6a·2AgOTf·0.5 *m*-xylene (17). The silver atom in this structure is coordinated to two **6a** molecules via two Ag–N bonds at distances of 2.14 and 2.14 Å and two triflate ions via two Ag–O bonds at distances of 2.49 and 2.50 Å. The overall coordination around the Ag atom is sawhorse-like with the two nitrogen atoms along the slightly bent horizontal bar and the two oxygen atoms at the fulcrum (O–Ag–O angle, 114.8°; N–Ag–N angle, 155.9°).

As Figure 1i shows, the structure consists of infinite chains of alternating **6a** molecules and Ag(I) ions, a structural motif also found in **9**–**11**. Triflate ions link these infinite chains into

pairs, as each triflate ion is coordinated to silver ions on two neighboring chains. The resultant coordination network is a double-stranded infinite chain. There are additional $\pi-\pi$ interactions both within each double-stranded chain and between the double chains. The closest $\pi-\pi$ distance is 3.6 Å, and the shortest Ag- π distance is 3.6 Å. Including these $\pi-\pi$ interactions the overall net structure is two-dimensional.

Single-Crystal Structure of $6a \cdot 2AgBF_4$ (18). There are two crystallographically non-equivalent Ag atoms in this structure. Each is coordinated to one nitrogen atom and three oxygen atoms in a sawhorse-like geometry. The Ag-N distances for Ag1 and Ag2 are 2.20 and 2.21 Å, respectively. The Ag-O distances for the two Ag atoms range from 2.30 to 2.61 Å.

The coordination network is very similar to that of **14**. The Ag1-**6a**-Ag2 units stack along *b* axis in a columnar structure, Figure 1j. Half of the side chains form linkages to intracolumnar Ag atoms, while half form intercolumnar linkages. The overall coordination network is therefore two-dimensional.

Single-Crystal Structure of $6a \cdot 1.25AgSbF_6 \cdot 1.25C_6H_6$ (19). **19** crystallized in the $P\bar{1}$ space group with a unit cell volume of over 17 000 Å³. In the final refinement, the aromatic rings of **6a** were restrained to be planar and the aromatic bonds of **6a** were restrained to all have the same bond length. The fluorine atoms of the SbF₆ anions related by pseudosymmetry were restrained to have the same anisotropic displacement parameters. Two-fifths of the silver atoms in the final structure (Ag2, Ag8, Ag9, and Ag3) are coordinated to one nitrogen and four oxygen atoms in a square pyramid with Ag-N distances ranging from 2.16 to 2.18 Å and Ag-O bonds from 2.36 to 2.61 Å. As Figure 2k shows, the remaining silver atoms are either coordinated in a linear fashion to two nitrogen atoms or are coordinated in a sawhorse-like geometry with two end nitrogen atoms at distances ranging from 2.10 to 2.18 Å and two fulcrum oxygen atoms at distances ranging from 2.54 to 2.69 Å.

As Figure 3c illustrates, a fundamental building block of this structure is a rigid rod, some 65 Å long with two end Ag atoms, each with only a single Ag-N bond and then alternating in the interior of the rod linear doubly coordinate **6a** molecules and silver sites. The overall rod contains a tetramer of **6a** molecules and two capping and three interior silver sites. Each of these tetrameric rods stacks parallel to one another to form a planar sheet with stacked π rings 3.8 Å apart. Neighboring tetramers stack in such a way as to place the end silver atoms in close proximity to more central aromatic rings of the neighboring tetramers. The end silver atoms are bonded to some of the oxygen atoms of the side chain of the neighboring tetramers. The overall coordination environment is therefore two-dimensional. Fairly large cavities are created by the staggered nature of adjacent tetramers. These cavities are in turn filled with solvent benzene molecules. The solvent benzene molecule lies parallel to the tetramer in such a way as to make $\pi-\pi$ distances of roughly 3.8 Å. This overall crystal structure may be viewed as intermediate between the doubly capped structures found for **12-16** and **18** and the infinite Ag-organic chains found for **9-11** and **17**.

Single-Crystal Structure of $5a \cdot AgOTf$ (20). The silver atom in this structure is trigonally coordinated to three **5a** molecules via three Ag-N bonds (all Ag-N distances, 2.24 Å). The triflate ion is weakly bonded at the apical position of a trigonal pyramid with a Ag-O distance of 2.51 Å.

As shown in Figure 2l, the crystal structure consists of slightly distorted honeycomb sheets based on alternating **5a** molecules and Ag(I) ions. The triflate ions lie on only one side of any

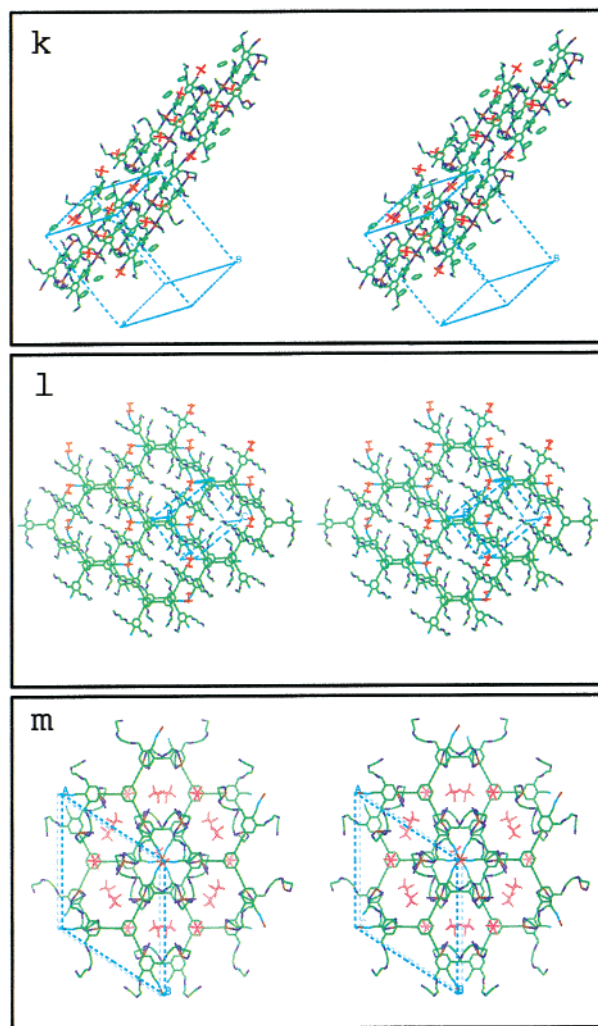


Figure 2. Stereoviews of crystal structures of (k) $6a \cdot 1.25AgSbF_6 \cdot 1.25C_6H_6$ (**19**), (l) $5a \cdot AgOTf$ (**20**), (m) $5b \cdot 4AgOTf$ (**21**). Counterions: red, Ag; brown, N; light blue, O; blue, C; green. For the sake of clarity, disorder in atom positions has been removed.

given sheet. The remaining side, unobstructed by the triflate ion, is $\pi-\pi$ stacked (interplanar distance, 3.3 Å) to another single sheet. The two sheets are so oriented that the silver atom of one sheet directly faces the central aromatic ring of the **5a** molecule of the other sheet. These bilayers thereafter stack ($\pi-\pi$ distance, 3.6 Å) so that the triflate ions lie at the corners of the hexagonal pores of a neighboring bilayer. The stacking of bilayers produces distorted hexagonal channels filled with the side chains and triflate ions. Considering only Ag-O and Ag-N bonds, the overall coordination network is two-dimensional. The inclusion of $\pi-\pi$ interaction results in a three-dimensional (3-D) structure.

Single-Crystal Structure of $5b \cdot 4AgOTf$ (21). The dataset for **21** proved to be of rhombohedral symmetry with systematic extinctions compatible with $R\bar{3}$, $R\bar{3}$, $R32$, $R3m$, and $R\bar{3}m$. The first two of these space groups have Laue class $\bar{3}$, while the last three have Laue class $3m$. As R_{int} was fairly uniform for all five space groups, we proceeded to solve the crystal structure in the higher Laue class. Initial refinement was carried out in $R\bar{3}m$. In this space group the rigid framework of the **5c** molecule as well as those of two silver sites could be located. The Ag1 site was three-coordinate to nitrogen in a trigonal planar fashion. Ag2 proved to be coordinated neither to the nitrogen atoms of **5c** nor to any triflate ions but instead only to the oxygen atoms derived from the side chains of **5c** molecules. Furthermore the

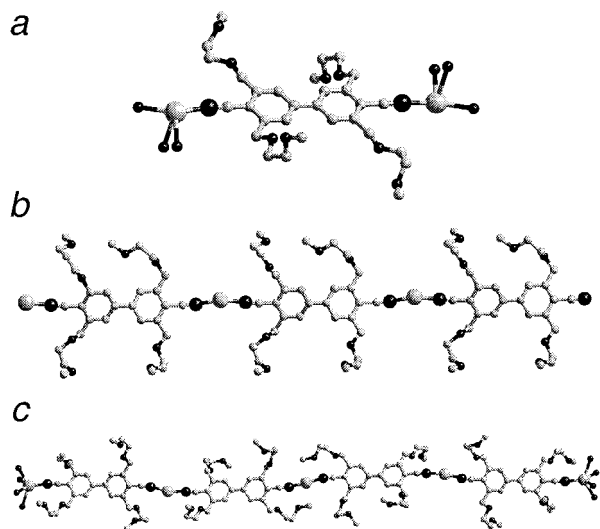


Figure 3. The three basic Ag–N concatenation motifs in **9–21**. (a) The monomeric unit in **6a**·2AgBF₄ (**18**). (b) The infinite chain in **6a**·2AgOTfA·0.5 *m*-xylene (**17**). (c) The tetrameric unit in **6a**·1.25AgSbF₆·1.25C₆H₆ (**19**). Ag: large gray, N: black medium, C: small gray, O: small black spheres.

Ag₂ site as well as one of the coordinating oxygen atoms lies on the mirror plane found in the $R\bar{3}m$ space group. Hence, the solution in $R\bar{3}m$ automatically leads to a complex disorder of the side chains around Ag₂. However, if one removes this mirror plane, lowering the space group to $R32$, all disorder of the side chains is removed. It therefore seemed preferable to finish the crystal structure refinement in $R32$. It should be noted that, as it is only the side chains of **5c** which break the $R\bar{3}m$ symmetry and as these side chains have atoms with large Debye–Waller factors, it is difficult to ascertain the correct space group. A less disordered model being preferable, we chose to refine this crystal structure in $R32$. All refinements in $R32$, $R\bar{3}$, or $R\bar{3}m$, however, bear the following geometric features in common.

The three 3-fold symmetric phenylacetylene arms of the molecule **5c** are capped by the Ag1 atom. Each Ag1 atom lies on a 6c site with C_3 symmetry and is coordinated to three nitrogen atoms at a bonding distance of 2.30 Å. The molecules **5c** together with the Ag1 atoms are therefore assembled into a honeycomb net with alternating vertices occupied by Ag1 atoms and the centroid aromatic rings of molecules **5c**. The oxygen atoms of the side chains are in turn coordinated to the Ag₂ site. Each Ag₂ site is coordinated to five oxygen atoms with Ag–O distances ranging from 2.46 to 2.72 Å. As Figure 2m shows, these side chains together with the Ag₂ sites form hexagonal rosettes whose center is the 3-fold symmetric Ag1 site. In the final refinement the side chain oxygen–carbon and carbon–carbon bond lengths were restrained to be respectively 1.43 and 1.53 Å.

There are three triflate sites in the crystal. Of these, two are disordered. Particularly complex is the disordered model chosen for the triflate ion nearest Ag1. These triflate ions lie between two Ag1 atoms with a distance from Ag1 to Ag1 of 7.32 Å. Furthermore, these Ag1 sites lie both on the same 3-fold axis. Were one to place the 3-fold axis of the triflate ion on this crystallographic 3-fold axis, due to the short Ag1–Ag1 distance, either the oxygen or the fluorine atoms of the triflate ions would approach Ag1 sites at chemically unreasonable distances. We found a chemically more reasonable solution, in which the 3-fold axis of the triflate ion is canted with respect to the crystallographic 3-fold axis. The result is a 6-fold disordered triflate ion with Ag1–O distances of 2.59 and 2.64 Å. A single one of

these disordered triflate ions is shown per site in Figure 2m. In the final refinement these disordered triflate ions were restrained to have a chemically reasonable triflate geometry.

Finally, it may be noted in Figure 2m that each of the hexagonal sheets lie parallel to one another. Interplanar distances alternate between 3.5 and 7.3 Å. The first distance is that generally expected for π – π aromatic interaction. Indeed, honeycomb nets separated at this shorter distance shows the typical slightly staggered parallel arrangement of aromatic rings. Such honeycomb nets are also paired up to form bilayers similar to those found in **21**. The 7.3 Å gap between neighboring bilayers is due to the larger spatial requirement of the tri(ethylene oxide) side chains.

Discussion

Crystal Structures. The 13 crystal structures reported above display a slightly bewildering array of crystal types. If we restrict our attention to the structures involving silver together with molecules **6a–b** and **8a–b**, molecules all with a rigid linear backbone capped at both ends with nitrile groups and also all with four oligo(ethylene oxide) chains pendant to this backbone, we find even here a real variation in structure. Considering Ag–N concatenation, the various units observed range from infinite chains of alternating organic molecules and silver ions as is found in **9–11** and **17** to oligomers as in **19**, to single organic molecules capped by Ag ions as in **12–16** and **18**. These three basic types are illustrated in Figure 3.

If in addition we add Ag–O coordination, there is an even greater range of structural variations. In **8a**·AgOTf (**9**), for example, the Ag–organic molecule infinite chains illustrated in Figure 3 are not cross-linked by any Ag–O bonds and the coordination network remains 1-D, while in the compositionally similar **8a**·AgPF₆ (**10**) similar infinite chains are linked together through Ag–O bonds to form a 2-D coordination network. Even less clear are the factors which cause **6b**·2AgBF₄·H₂O (**14**) to have a 2-D coordination network and yet the slightly more silver-rich **6b**·AgBF₄·C₆H₆·H₂O (**15**) to be 1-D. In the case of the latter two compounds, both systems have a rich environment of Ag–O bonds. However, for **15** these Ag–O bonds are between organic molecules and silver atoms already connected through the Ag–N-based infinite chains, while for **14** these Ag–O bonds bridge adjacent Ag–N-based infinite chains to each other.

This is not to say that one cannot *a posteriori* rationalize these structural results. To a good extent one can. The following rules generally hold. The chief factor in the crystal topologies is the Ag–N coordination. If each Ag is coordinated to only a single N then perforce the structure will contain Ag–organic molecule–Ag monomer units. This is the case in **12–16** and **18**. If, however, the Ag atoms are two-coordinate to nitrogen atoms, the Ag–N coordination environment is linear, and the resulting structures contain infinite chains of alternating silver atoms and organic molecules. This is the case in **9–11** and **17**. The determining factor as to whether one or the other environment is adopted appears to be the stoichiometric ratios of silver ions to organic molecules. In the infinite chain structures **9–11** and **17**, this ratio is 1:1 while for the monomeric structures the ratio is always greater than 2:1. Only in the case of intermediate stoichiometry as is found in the 5:4 ratio of **19** does one find the intermediate tetrameric structure.

These results suggest that, as may be expected, the strongest coordination bonds in these systems are between silver and nitrogen. All nitrogen atoms are therefore coordinated to silver

atoms. As such, a one-to-one ratio of silver ions to the ditopic ligands **6a–b** and **8a–b** results in an average silver-to-nitrogen coordination of two. The linear N–Ag–N is the coordination geometry lowest in energy, and disproportionation of the silver–nitrogen linkage does not occur. As molecules **6a–b** and **8a–b** are themselves linear, the result is the formation of infinite chains of alternating ligands and silver ions. Similarly, there is energetic preference for two silver atoms singly bonded to nitrogen rather than one silver atom two-coordinate to nitrogen. Therefore, when organic molecule-to-silver ratios exceed 1-to-2, one finds monomeric units rather than more complicated structures.

The dimensionality of the coordination network is further complicated by the Ag–O bonds. The following two general rules, however, hold. If the number of side chain oxygen atoms is greater, as is found in molecules **6b** and **8b**, as opposed to **6a** and **8a**, then the overall coordination network is 1-D rather than 2-D. Also if the crystal contains coordinating counterions such as the triflate ions or adventitious water, one finds 1-D networks. Thus, **9**, **12–13**, and **15–17** all contain either the long side chain molecules **6b** or **8b**, a triflate ion, or water molecules and have 1-D coordination networks, while **10–11**, **14**, and **18–19** contain none of the above molecular units and have 2-D coordination networks. The only exception to this general rule is the crystal structure **14**, and here the exception is caused by a disordered water molecule which has only been tentatively assigned as such.

We may account for these trends in the following way. As described previously, Ag–N coordination by itself leads to the formation of monomeric, tetrameric units or linear infinite chains. Hence, whether the overall coordination is one or two-dimensional depends on the Ag–O linkages. Both the oxygen atoms of the triflate ion and the water molecules form stronger bonds to the silver ions and hence they preferentially coordinate to the metal atoms over the ether oxygen atoms of the various organic side chains. As stronger bonds are formed, there tend to be fewer Ag–O bonds in these former systems, and as these oxygen atoms do not have to bridge the silver atom the new organic ligands, they do not cause an increase in the dimensionality of the coordination network. Similarly the more oxygen-rich molecules **6b** and **8b** are able each by themselves to more readily satisfy the coordination requirements of the silver ions. A single **6b** or **8b** can furnish two or three coordinating oxygen atoms, again reducing the need for Ag ions to further cross-link to other organic molecules. Again, the result is a reduced dimensional system.

Interfacial Model. The goal of systematic structural studies is however not just the rationalization of determined structures but also the prediction of structural properties in new as yet undetermined families of structures. It is here that we can see a breakdown of the aforementioned generalizations. For example, if we were to substitute for the silver ions another metal ion, introduce a kink in the rigid backbone of the phenylacetylene unit, or even just extend the side chains to a significantly longer length, it would be difficult for us to predict even the dimensionality of the overall coordination network. Predictions we can make with confidence are of a simpler sort. Consider, for example, the heretofore unprepared **8b**·AgOTf or **6a**·2AgPF₆. Following our previously established rules, we expect for the former compound a structure with an infinite linear chain of **8b**–Ag ions and an overall 1-D coordination network of Ag–N and Ag–O bonds. In the latter system we expect a compound composed of Ag–**6a**–Ag monomeric units linked together by Ag–O bonds into a 2-D network.

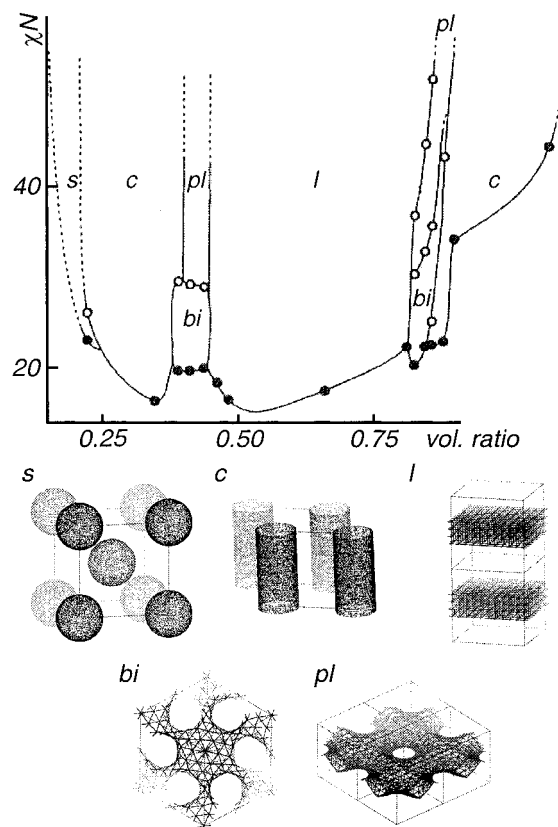


Figure 4. Experimentally determined phase diagram for PS–PI (polystyrene–polyisoprene)diblock copolymers.⁸⁶ s: spheres, c: columns, l: layers, bi: bicontinuous, pl: perforated layers.

In these examples, we can predict with some confidence as we interpolate between existing results. Where our predictive powers break down is where we need to extrapolate to significantly new crystal types. Our rules discussed so far allow the former and not the latter type of predictions.

In recent years, however, just such an extrapolative scheme has been developed for large-length scale heterogeneous molecules as are found in amphiphilic and block copolymer systems.^{92–94} The types of systems studied involve mixtures of two different chemical components. Components are chosen which on their own would phase-separate. However, by the addition of amphiphilic surfactants or by the direct joining of the two different polymer types, a mixture of the two components is enforced. It has been found in such cases that an almost universal phase diagram is produced.^{89,93} Key factors are the volume ratio of the two components and the driving force of segregation, usually characterized by the parameter χN .⁹⁵ A typical example is shown in Figure 4.

At low volume ratios, spheres of one component form inside the main body of the second body. At slightly higher volume ratios, the spheres turn into columns, while at the volume ratio of 1:1 lamellar structures are found. Finally, between the columnar and lamellar regions a more complex type of structure appears, involving either a bicontinuous form or a perforated layer structure. Principal driving forces for this structure map

(92) Thomas, E. L.; Lescanec, R. L. Phase Morphology in Block Copolymer Systems. In *Self-order and Form in Polymeric Materials*; Keller, A., Warner, M., Eds.; Chapman & Hall: London, 1995; Chapter 10.

(93) Hamley, I. W. *The Physics of Block Copolymers*; Oxford University Press: New York, 1998.

(94) Diele, S.; Brand, P.; Sackmann, H. *Mol. Cryst. Liq. Cryst.* **1972**, *17*, 163.

(95) Bates, F. S.; Fredrickson, G. H. *Annu. Rev. Phys. Chem.* **1990**, *41*, 525.

are the minimization of the interfacial area between the two chemical components or alternatively the curvature requirements of this interface.

To date very little effort has been spent to see if this overall general map is useful in the prediction and rationalization of extended networks in coordination solids although significant efforts have been made to apply the concepts of minimal surfaces to solid-state crystal chemistry.^{96–99} Nor at the outset is it clear that this generic framework will be useful for extended coordination networks. The type of systems studied to date have been at nanometer scales ranging up to 1000 Å in unit cell axes. At such large distances, the individual vagaries caused by anisotropic chemical bonds will be minimized. As we approach 5–10 Å, the typical unit cell lengths found in many extended coordination networks, even the concept of the interface is less well defined. Nevertheless, many coordination networks continue to adopt structures reminiscent of those found in Figure 4.^{49,70,100–113}

We have prepared the crystals **9–21** in order to test the utility of this generic framework (see Table 1). In each of the crystallized extended networks, the organic molecules clearly divide into a phenylacetylene backbone which is strongly hydrophobic and oligo(ethylene oxide) side chains which are correspondingly hydrophilic. Joining these molecules together are silver salts. While the anion portion of the salt is certainly hydrophilic, the case of the silver ion is less clear. Silver ions coordinated solely to oxygen atoms are acting in a hydrophilic manner. However, silver ions bound to softer ligands such as nitrile groups and which in addition show weak bonding to π -aromatic clouds are less hydrophilic. We will consider the first sort of silver ions to be hydrophilic and the latter to be intermediate in their hydroaffinity. Similarly, we will consider nitrile groups to be of intermediate hydrophilicity. As for the included benzene and water molecules, they are treated as hydrophobic and hydrophilic, respectively. In the Figures 5 and 6 we redisplay these 13 structures using green to indicate the hydrophilic portions of the crystal, red for hydrophobic portions, and brown for those portions intermediate in hydroaffinity.

The 13 structures divide into three basic families. For **12–14, 16, and 18** we find columns of the hydrophobic moieties in a mixture of hydrophilic groups. For **9–11, 15, 17, and 21**, there

are layers of alternating hydrophobic and hydrophilic ligands. Finally, **19** and **20** are bicontinuous. In the case of **20**, we find columns of hydrophilic moieties partially separated by a pseudo-hexagonal network of hydrophobic aromatic groups. However, the hydrophilic columns are not isolated but are in close contact with one another. In the case of **19**, the structure is lamellar, but again there are close contacts between all next nearest neighbor layers through perforations in each individual lamella. For both **20** and **19**, the result of these closest contacts are the formation of one continuous hydrophobic and one continuous hydrophilic domain. In accordance with the literature, they are therefore termed bicontinuous.^{114,115}

It may be seen that all 13 structures have topologies in correspondence with the generic structures previously shown in Figure 4. Of course, in comparing Figure 4 to Figures 5 and 6 there are noticeable differences. In Figure 3, the columnar structure has only two lattice axes and the layer structure, only a single lattice axis, while in Figures 5 and 6 all of the structures correspond to normal crystal unit cells with three cell axes and three cell angles. Furthermore, in Figure 4 the columnar structure has hexagonal symmetry, while in Figure 5 this 6-fold symmetry is lost. Even more complex are the bicontinuous systems. Here, in the block copolymer literature, tremendous effort is made to distinguish between different bicontinuous systems such as the gyroid and the double diamond forms.^{116–118} If crystal symmetry is no longer preserved, the boundaries become more indistinct. Rather than trying to keep these different groups separate, in Figure 5 we topologically group them into a single bicontinuous family. Nevertheless, the correspondence between the crystal structures reported in this work and the crystal topologies found for generic biphasic heterogeneous systems is striking.

If the overall picture of biphasic separation is to prove useful, we need to find the factors which cause the columnar, lamellar, or bicontinuous topologies. As mentioned earlier, it is thought that the two chief factors are the volume ratios and the overall energy of segregation. In our case we are dealing with highly hydrophobic aromatic rings and equally hydrophilic oligo(ethylene oxide) moieties. We are clearly within the high segregation limit. We therefore turn to the hydrophilic-to-hydrophobic ratio. At the same time we need to choose a useful algorithm to rigorously classify a given crystal as of columnar, lamellar, perforated lamellar, or bicontinuous type.

We chose the following method for calculating volume ratios. We consider first the hydrophilic atoms. We place at each hydrophilic atom a sphere with a radius corresponding to the given atom's van der Waals radius and calculate the volume of the union of these spheres (The van der Waals radii are standard⁹¹ and are given in the Supporting Information). We carry out the same procedure for the hydrophobic atoms. We then take the ratio of the two volumes. To verify that our findings are invariant to reasonable definitions of hydrophobicity and hydrophilicity, we performed these same calculations under a range of assumptions. In particular we considered the carbon adjacent to both the aromatic rings and the first oxygen of the side chain to be hydrophobic in one set of calculations and hydrophilic in another. As for the nitrile groups and the silver ions bonded to nitrile groups, we considered them both

(96) von Schnering, H. G.; Nesper, R. *Angew. Chem., Int. Ed. Engl.* **1987**, *26*, 1059.

(97) Anderson, S. *Angew. Chem., Int. Ed. Engl.* **1983**, *22*, 69.

(98) Hyde, S. T.; Anderson, S. Z. *Kristallogr.* **1986**, *174*, 225.

(99) Nesper, R. *Angew. Chem., Int. Ed. Engl.* **1991**, *30*, 789.

(100) Bonavia, G.; Haushalter, R. C.; O'Connor, C. J.; Sangregorio, C.; Zubieta, J. *Chem. Commun.* **1998**, 2187.

(101) Shimizu, G. K. H.; Enright, G. D.; Ratcliffe, C. I.; Ripmeester, J. A.; Wayner, D. D. M. *Angew. Chem., Int. Ed.* **1998**, *37*, 1407.

(102) Choi, H. J.; Suh, M. P. *J. Am. Chem. Soc.* **1998**, *120*, 10622.

(103) Bu, X.; Feng, P.; Stucky, G. D. *Chem. Mater.* **1999**, *11*, 3423.

(104) Livage, C.; Egger, C.; Férey, G. *Chem. Mater.* **1999**, *11*, 1546.

(105) Shan, Y.; Huang, R. H.; Huang, S. D. *Angew. Chem., Int. Ed.* **1999**, *38*, 1751.

(106) Niu, T.; Wang, X.; Jacobson, A. J. *Angew. Chem., Int. Ed.* **1999**, *38*, 1934.

(107) Johal, M. S.; Cao, Y. W.; Chai, X. D.; Smilowitz, L. B.; Robinson, J. M.; Li, T. J.; McBranch, D.; Li, D. *Chem. Mater.* **1999**, *11*, 1962.

(108) Lin, K. J. *Angew. Chem., Int. Ed.* **1999**, *38*, 2730.

(109) Haskouri, J. E.; Roca, M.; Cabrera, S.; Alamo, J.; Beltrán-Porter, A.; Beltrán-Porter, D.; Marcos, M. D.; Amorós, P. *Chem. Mater.* **1999**, *11*, 1446.

(110) Natarajan, S.; Vaidyanathan, R.; Rao, C. N. R.; Ayyappan, S.; Cheetham, A. K. *Chem. Mater.* **1999**, *11*, 1633.

(111) Grey, I. E.; Hardie, M. J.; Ness, T. J.; Ratson, C. L. *Chem. Commun.* **1999**, 1139.

(112) Orr, G. W.; Barbour, L. J.; Atwood, J. L. *Science* **1999**, *285*, 1049.

(113) Comotti, A.; Simonutti, R.; Gatel, G.; Sozzani, P. *Chem. Mater.* **1999**, *11*, 1476.

(114) Longley, W.; McIntosh, T. J. *Nature (London)* **1983**, *303*, 612.

(115) Thomas, E. L.; Anderson, D. M.; Henke, C. S.; Hoffman, D. *Nature (London)* **1988**, *334*, 598.

(116) Luzzati, V.; Spet, P. A. *Nature (London)* **1967**, *215*, 701.

(117) Förster, S.; Khandpur, A. K.; Zhao, J.; Bates, F. S.; Hamley, I. W.; Ryan, A. J.; Bras, W. *Macromolecules* **1994**, *27*, 6922.

(118) Hajduk, D. A.; Harper, P. E.; Gruner, S. M.; Kim, C. C. H. G.; Thomas, E. L.; Fetters, L. J. *Macromolecules* **1994**, *27*, 4063.

Table 1. Crystal Data and Structure Refinements for Compounds 9–21

	9	10	11	12	
formula	C ₃₃ H ₄₀ AgF ₃ N ₂ O ₁₁ S	C ₃₂ H ₄₀ AgF ₆ N ₂ O ₈ P	C ₃₂ H ₄₀ AgF ₆ N ₂ O ₈ Sb	C ₄₀ H ₅₈ Ag ₂ F ₁₂ N ₂ O ₁₃ Sb ₂	
mol wt	837.60	833.50	924.28	1462.12	
T (K)	173(2)	173(2)	173(2)	173(2)	
wavelength (Å)	0.71073	0.71073	0.71073	0.71073	
system	triclinic	triclinic	triclinic	monoclinic	
space group	P1	P1	P1	P2 ₁ /n	
a (Å)	8.0147(1)	11.2529(2)	11.3394(3)	13.5024(6)	
b (Å)	15.1807(1)	13.4468(2)	12.231	9.8307(4)	
c (Å)	15.93250(1)	14.1345(2)	15.0405(4)	38.919(2)	
α (deg)	108.696(1)	104.016(1)	101.335(1)	90	
β (deg)	98.906(1)	104.434(1)	110.647(2)	94.853(1)	
γ (deg)	93.080(1)	111.615(1)	106.036(1)	90	
V (Å ³)	1802.96(3)	1788.19(5)	1773.09(7)	5147.6(4)	
Z	2	2	2	4	
ρ _{calc} (g/cm ³)	1.543	1.548	1.731	1.887	
abs coeff (mm ⁻¹)	0.693	0.690	1.397	1.891	
θ range (deg)	2.28–23.26	1.75–23.26	1.83–18.84	2.10–26.37	
limiting indices	–8 ≤ h ≤ 8 –16 ≤ k ≤ 16 –17 ≤ l ≤ 10	–12 ≤ h ≤ 12 –12 ≤ k ≤ 14 –15 ≤ l ≤ 15	–10 ≤ h ≤ 8 –11 ≤ k ≤ 11 –13 ≤ l ≤ 13	–16 ≤ h ≤ 14 –12 ≤ k ≤ 9 –45 ≤ l ≤ 48	
data/restraints/params	5093/0/448	5060/0/451	2741/0/241	10422/0/642	
measd reflns	8718	8092	4924	28323	
unique reflns	5093	5060	2741	10422	
abs correction	SADABS	SADABS	SADABS	SADABS	
GOF on F ²	1.006	1.062	1.731	0.891	
R _{int}	0.0461	0.0357	0.0735	0.0683	
R1	0.0587 (I > 2σ(I))	0.060 (I > 2σ(I))	0.1084 (I > 2σ(I))	0.0411 (I > 2σ(I))	
wR2	0.1515 (I > 2σ(I))	0.1574 (I > 2σ(I))	0.2942 (I > 2σ(I))	0.0949 (I > 2σ(I))	
	13	14	15	16	
formula	C ₂₁ H ₂₈ Ag ₂ F ₆ NO ₁₂ S ₂	C ₃₈ H ₅₆ Ag ₂ B ₂ F ₈ N ₂ O ₁₃	C ₄₄ H ₆₄ Ag ₃ B ₃ F ₁₂ N ₂ O ₁₃	C ₁₉ H ₂₈ AgF ₆ NO ₆ Sb	
mol wt	880.30	1138.21	1413.01	710.04	
T (K)	173(2)	173(2)	173(2)	173(2)	
wavelength (Å)	0.71073	0.71073	0.71073	0.71073	
system	monoclinic	monoclinic	triclinic	monoclinic	
space group	P2 ₁ /n	P2 ₁ /n	P1	C2/c	
a (Å)	7.3265(3)	17.709(1)	12.3839(2)	24.744(2)	
b (Å)	26.101(1)	7.5134(6)	14.4048(2)	7.3484(7)	
c (Å)	15.9343(3)	18.067(1)	16.5943(3)	27.940(3)	
α (deg)	90	90	104.869(1)	90	
β (deg)	94.473(2)	110.527(2)	99.550(1)	91.706(2)	
γ (deg)	90	90	99.507(1)	90	
V (Å ³)	3037.8(2)	2251.2(3)	2753.61(8)	5077.9(8)	
Z	4	2	2	8	
ρ _{calc} (g/cm ³)	1.925	1.679	1.704	1.858	
abs coeff (mm ⁻¹)	1.522	0.966	1.157	1.913	
θ range (deg)	2.02–20.82	2.00–23.25	1.50–20.81	2.17–24.80	
limiting indices	–7 ≤ h ≤ 7 –26 ≤ k ≤ 25 –11 ≤ l ≤ 15	–19 ≤ h ≤ 18 –8 ≤ k ≤ 8 –15 ≤ l ≤ 20	–12 ≤ h ≤ 12 –12 ≤ k ≤ 14 –16 ≤ l ≤ 13	–17 ≤ h ≤ 28 –8 ≤ k ≤ 8 –32 ≤ l ≤ 32	
data/restraints/params	3176/0/227	3213/9/320	5680/0/684	4309/0/307	
measd reflns	9836	8778	9610	11867	
unique reflns	3176	3213	5680	4309	
abs correction	SADABS	SADABS	SADABS	SADABS	
GOF on F ²	1.181	0.989	0.976	1.048	
R _{int}	0.1151	0.0823	0.0537	0.0893	
R1	0.0784 (I > 2σ(I))	0.0587 (I > 2σ(I))	0.0587 (I > 2σ(I))	0.0626 (I > 2σ(I))	
wR2	0.1949 (I > 2σ(I))	0.1261 (I > 2σ(I))	0.1345 (I > 2σ(I))	0.0873 (I > 2σ(I))	
	17	18	19	20	21
formula	C ₃₅ H ₄₅ AgF ₃ N ₂ O ₁₁ S	C ₃₀ H ₄₀ Ag ₂ B ₂ F ₈ N ₂ O ₈	C ₃₀₀ H ₃₈₀ Ag ₁₀ F ₆₀ N ₁₆ O ₆₄ Sb ₁₀	C ₅₈ H ₅₉ AgF ₃ N ₃ O ₁₅ S	C ₈₅ H ₁₁₁ Ag ₄ F ₁₂ N ₃ O ₃₆ S ₄
mol wt	866.66	946.00	8670.40	1235.01	2538.49
T (K)	173(2)	173(2)	173(2)	173(2)	173(2)
wavelength (Å)	0.71073	0.71073	0.71073	0.71073	0.71073
system	triclinic	monoclinic	triclinic	triclinic	rhombohedral
space group	P1	P2 ₁ /c	P1	P1	R32
a (Å)	8.7526(6)	17.4924(6)	19.4111(3)	8.7564(1)	22.4670(4)
b (Å)	14.835(1)	7.1943(1)	27.8506(4)	18.2486(2)	22.4670(4)
c (Å)	15.073(1)	28.4848(9)	33.0801(3)	19.5099(3)	36.1131(5)
α (deg)	97.790(2)	90	98.636(1)	104.3780(2)	90
β (deg)	97.586(2)	95.601(2)	91.473(1)	99.1780(7)	90
γ (deg)	92.184(2)	90	102.486(1)	102.2930(8)	120
V (Å ³)	1919.0(2)	3567.6(2)	17231.2(4)	2875.40(6)	15786.5(5)
Z	2	4	2	2	6

Table 1. (Continued)

	17	18	19	20	21
ρ_{calc} (g/cm ³)	1.500	1.761	1.671	1.426	1.602
abs coeff (mm ⁻¹)	0.654	1.190	1.427	0.466	0.915
θ range (deg)	2.35–20.82	1.17–20.82	0.62–19.78	1.11–24.71	1.54–23.26
limiting indices	$-8 \leq h \leq 8$	$-17 \leq h \leq 13$	$-18 \leq h \leq 17$	$-10 \leq h \leq 10$	$-24 \leq h \leq 17$
	$-14 \leq k \leq 13$	$-7 \leq k \leq 7$	$-26 \leq k \leq 18$	$-21 \leq k \leq 14$	$-24 \leq k \leq 24$
	$-15 \leq l \leq 15$	$-26 \leq l \leq 28$	$-30 \leq l \leq 31$	$-22 \leq l \leq 22$	$-34 \leq l \leq 40$
data/restraints/params	3910/18/303	3715/0/259	30210/4636/1968	9561/0/428	5051/157/245
measd reflns	7119	11485	51478	14621	20721
unique reflns	3910	3715	30210	9561	5051
abs correction	SADABS	SADABS	SADABS	SADABS	SADABS
GOF on F^2	1.070	1.039	1.197	1.173	2.334
R_{int}	0.1306	0.0885	0.0751	0.0379	0.0742
R1	0.1063 ($I > 2\sigma(I)$)	0.0952 ($I > 2\sigma(I)$)	0.1352 ($I > 2\sigma(I)$)	0.0653 ($I > 2\sigma(I)$)	0.1564 ($I > 2\sigma(I)$)
wR2	0.2515 ($I > 2\sigma(I)$)	0.2270 ($I > 2\sigma(I)$)	0.3619 ($I > 2\sigma(I)$)	0.1678 ($I > 2\sigma(I)$)	0.3684 ($I > 2\sigma(I)$)

^a $R1 = \sum ||F_c| - |F_o|| / \sum |F_o|$. ^b $wR2 = [\sum [w(F_o^2 - F_c^2)]^2 / \sum [w(F_o^2)]^2]^{1/2}$.

hydrophobic and of intermediate character (in this latter case they are not considered in either volume grouping).

As a final test, we created de novo models for the molecules and ions found in each crystal structure. Bond distances are standard¹¹⁹ and are given in the Supporting Information. sp^3 , sp^2 , and sp sites were assumed to be respectively perfectly tetrahedral, trigonal planar, and linear. These latter calculations therefore did not rely on crystal data beyond knowledge of the unit cell chemical composition. In columns A and D of Table 2, we compare the volume ratios found from both the molecular models and actual crystal data. We assumed in both cases that all sp^3 carbon atoms adjacent to oxygen atoms are hydrophilic and the CN–Ag units are hydrophobic. As may be seen, the volume ratios obtained from molecular composition and crystal structure are in substantial agreement.

Deviation is greatest for **21**. Crystal **21** is in many ways the weakest crystal solution reported in this paper with an R1 and wR2 of respectively 15.6 and 36.8%. Several of the outermost side chain atoms could not be located in the structure, nor with such large Debye–Waller factors were any solvent molecules found. Therefore, both exact molecular composition of the unit cell and locations of the exact oligo(ethylene oxide) side chains are undetermined. The difference in the two calculations represents the uncertainty as to the actual hydrophilic-to-hydrophobic volume ratio.

We now turn to the assignment of structure topology. This proved to be somewhat difficult. At first, one might think that we need only examine the surfaces of the two components derived by the above volume calculations. However, such surfaces are often very complex. The complexity may be understood when we recall that the Kitaigorodsky ratio, that is, the ratio between the portion of the cell occupied by the atoms and the volume of the unit cell itself, generally lies between 70 and 75%.¹²⁰ Some quarter of the cell volume belongs neither to the hydrophobic or hydrophilic portions. It is presumably this 25% void which greatly adds to the complexity of the overall surface morphology.

Much more useful has proven to be close contacts between neighboring atoms. In the case of a columnar structure, the minor component, which constitutes the columns themselves, should not have closest contacts between neighboring column atoms. Similarly, in the lamellar structures neither component should have close contacts which traverse the complementary layer. In the perforated layer structure one of the two components

should have closest contacts between layers, while the other component should not. Finally, in bicontinuous systems, both components should by themselves form one continuous domain. The only undetermined factor is the definition of the closest contact itself. Here again we based our definition on van der Waals radii. While the sum of the van der Waals radii prove slightly too small for this purpose, if we choose a close contact distance as being one less than 1.15 to 1.30 times the sum of the two atoms' van der Waals radii, the resulting structure assignments correspond to the structure type which is expected by visual inspection. Furthermore, only 10% of the structures change their classification in changing the cutoff parameter from 1.15 to 1.30.

In Table 2 we list under a variety of different definitions of hydrophilicity, hydrophobicity and close contact, the breakdown of structure type as a function of hydrophilic to hydrophobic volume ratios. As may be seen under each of these different definitions, the hydrophilic to hydrophobic volume ratio proves to be a critical component in separating columnar- from layer-type structures.

For example in choosing sp^3 carbon atoms adjacent to the aromatic rings to be hydrophilic and CN–Ag units to be hydrophobic, we find four distinct regions of structure type. We find for volume ratios between 21 to 28% columnar structures, from 29 to 34% a combination of columnar and perforated layer structures, from 35 to 38% layer structures, and finally at 40% bicontinuous structures. Similar evolution of structure type as a function of volume ratios is found for each alternate definition of hydroaffinity. As may be seen in Table 2, the predominant change due to alternate definitions of hydroaffinity is not in the separation of structure types but the actual numerical value assigned to the volume ratios. With the exception of **18** and possibly **21** one may correctly order the 13 structures by volume ratio from columnar, to lamellar, to bicontinuous structures. For **18** this exception depends on the exact definition of hydroaffinity. If we define the sp^3 carbon atoms adjacent to the aromatic rings to be hydrophobic, **18** converts from columnar to the perforated layer type and is no longer exceptional. This picture is confirmed by Figure 5f, in which it may be seen that **18** is poised between the columnar and lamellar types. For crystal **21**, the volume ratio on the crystal data places this perforated layer structure near the volume ratio of the other perforated layer structure, **15**. The molecular model data strongly suggests that this volume ratio is significantly lower in value; we discuss this point further below.

Figure 5 illustrates nicely the overall evolution of structures. We have ordered the 12 structures in Figure 5 by their hydrophobic-to-hydrophilic volume ratios. In Figure 5a the

(119) March, J. *Advanced Organic Chemistry*, 4th ed.; Wiley: New York, 1992; p 21.

(120) Kitaigorodsky, A. I. *Molecular Crystals and Molecules*; Academic Press: Inc.: New York, 1973; pp 18–21.

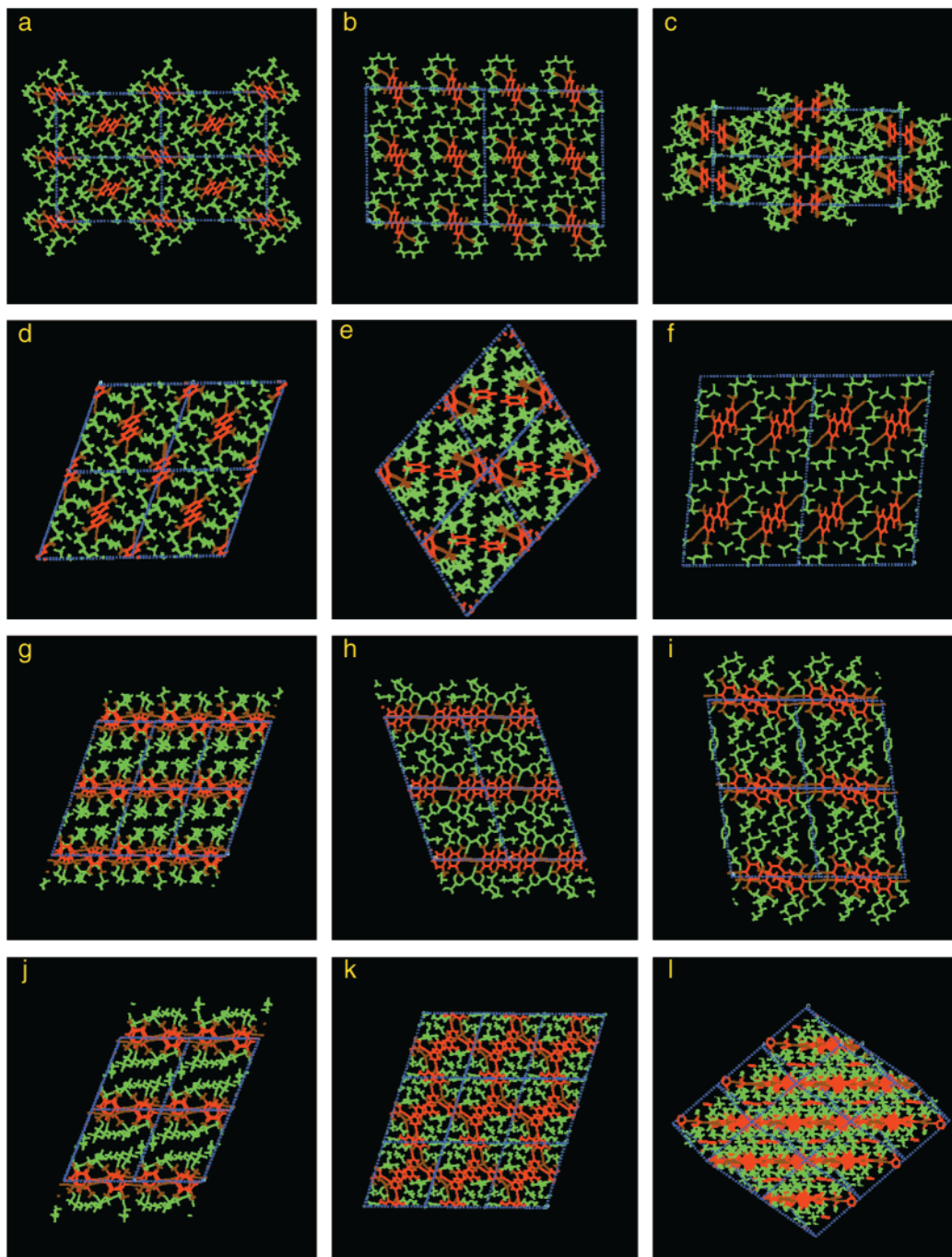


Figure 5. Hydrophobic and hydrophilic portions of **9–20**. (a) **13**. (b) **16**. (c) **12**. (d) **14**. (e) **15**. (f) **18**. (g) **11**. (h) **9**. (i) **17**. (j) **10**. (k) **20**. (l) **19**. Structures are ordered in increasing hydrophobicity. Red: hydrophobic, green: hydrophilic, brown: intermediate. See text for definitions of hydroaffinity.

pseudo-hexagonal columns of the hydrophobic portion of **13** are clear. As we increase this volume ratio these columns begin to approach one another, until by Figure 5, parts e and f, the perforated layers are evidenced. At higher volume ratios true layer structures are found until at even higher ratios bicontinuous structures appear. Taken together one sees isolated hydrophobic channels grow in size until they become sufficiently large, and it is the hydrophilic portions which begin to form in more isolated pockets.

Of particular interest are structures **20** and **21**. Unlike the structures previously discussed, the rigid phenylacetylene backbones in these crystals arise from 3-fold symmetric planar groups. In each organic molecule there are three rigid phenylacetylene groups extending out from the central aromatic ring

and each of these three groups is capped with a nitrile group. We have recently shown that such molecules tend to enforce a 3-fold trigonal planar coordination environment for the silver ions and that this combination of 3-fold symmetric silver ions and 3-fold symmetric organic molecules leads to a honeycomb pattern in which the walls of the channel are derived from a phenylacetylene–silver network and the interior of the channels contain cocrystallized solvent molecules. References 24, 25, and 44 contain some 20 examples of this pattern. The distinct energetic preference is therefore for the columnar-type structure, where the columns are composed of solvent molecules and the matrix is the phenylacetylene–silver host.

In **20** and **21** we have further attached six oligo(ethylene oxide) side chains to the phenylacetylene backbone. In these

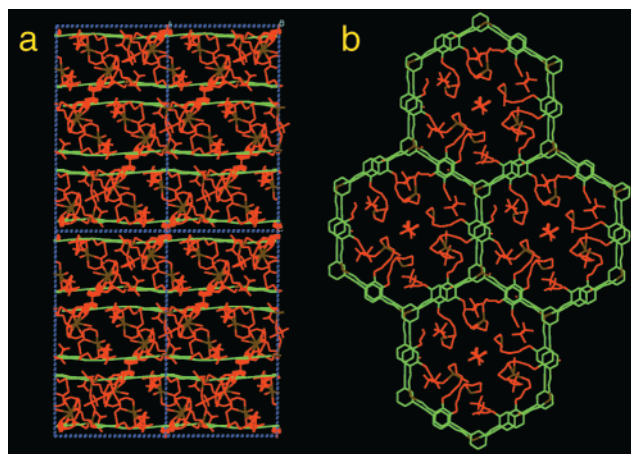


Figure 6. Hydrophobic and hydrophilic portions of **5b**·4AgOTf (**21**). (a) View down the [1 0 0] direction. (b) View down the *c* axis of a single bilayer perforated by hydrophilic moieties. Red: hydrophilic, green: hydrophobic, brown: intermediate. See text for definitions of hydroaffinity.

Table 2. Topologies of Compounds **9**–**21** under Different Definitions of Hydrophilicity and Hydrophobicity

compd	A ^a		B ^b		C ^c		D ^d
	vol ratio (%)	topology ^e	vol ratio (%)	topology	vol ratio (%)	topology	vol ratio (%)
13	21.0	C	26.2	C	15.7	C	20.6
16	23.6	C	30.6	C	17.1	C	24.9
12	26.0	C	32.8	C	20.4	C	26.3
14	26.9	C	33.0	C	19.4	C	26.5
21	29.0	PL	34.7	PL	25.0	PL	23.5
15	30.5	PL	37.9	PL	25.2	PL	30.8
18	34.3	C	40.0	PL	26.0	C	33.5
11	34.8	L	44.6	L	29.0	L	34.9
9	34.9	L	44.3	L	28.4	L	35.1
17	35.9	L	43.1	L	31.2	L	37.1
10	36.0	L	45.9	L	29.8	L	35.3
20	39.7	BI	49.1	IC	35.3	BI	40.6
19	41.0	BI	48.7	BI	35.6	BI	40.3

^a sp³ carbon atoms next to aromatics: hydrophilic; CN–Ag units: hydrophobic; data: crystal structure. ^b sp³ carbons next to aromatics: hydrophobic; CN–Ag units: hydrophobic; data: crystal structure. ^c sp³ carbons next to aromatics: hydrophilic; CN–Ag units: intermediate; data: crystal structure. ^d sp³ carbon atoms next to aromatics: hydrophilic; CN–Ag units: hydrophobic; data: molecular model. ^e Closest contacts are set at 1.15 times the sum of van der Waals radii. C: column, PL: perforated layer, L: layer, BI: bicontinuous, IC: inverse column.

systems we are therefore able to partially control the amount of material outside the original honeycomb phenylacetylene matrix. For **20**, the honeycomb structure is sufficiently capacious to allow all the mono(ethylene oxide) side chains to lie within the channels. Hence, the original solvent-based columnar structure is retained. For **21**, the tri(ethylene oxide) side chains are too large and the honeycomb channels split apart into bilayer hexagonal sheets with the excess side chain molecules filling the layer between these sheets. In Figures 2 and 6 we show views of the bilayers for both **20** and **21**. The side chains are safely contained within the channel in **20** but are excessively large for **21**. Structures **20** and **21** are thus crystals where the trigonal planar nature of both the ligands and metal ions highly restrict the possible crystalline topologies. It is therefore unclear whether these structures will conform to the interfacial model described above.

In **20** the volume ratio in column A of Table 2 is 40%. The local geometry requirements point to a hexagonal columnar structure with hydrophilic regions separated by a hydrophobic matrix. As Figure 4 shows these two requirements do not seem

compatible. The crystal structure resolves this difference by forming close contacts between columns. The resultant perforated columnar structure is therefore bicontinuous, a structure-type much more compatible with the 40% volume ratio. Interestingly, the other crystal with an equally high volume ratio, **19**, also forms a bicontinuous structure, but here the bicontinuous domains are based on a lamellar structure in which each layer type is perforated to allow for close contacts.

For **21** the volume ratio is either 29% (column A, Table 2), quite near the crossover from the columnar to lamellar structure type, or 24% > (column D, Table 2), more properly in the columnar region of structures. The local geometry requirements of 3-fold coordination planar molecules and 3-fold coordinate silver ions is not compatible with the columnar structure. **21** forms in the perforated layer structure, a structure expected to be found near the crossover point.

It is interesting to speculate what would occur if one really opposed local geometry requirements to overall surface area issues. We can think of two such limiting cases. If we were to prepare a linear phenylacetylene nitrile compounds with extremely long oligo(ethylene oxide) side chains, we could prepare systems with extremely low volume ratios, but for which the local π – π stacking forces would favor the continued formation of π -stacked columns.¹²¹ While Figure 4 would suggest the formation of a spherical structure, there is a good likelihood that a columnar structure would still be maintained. Similarly, if side chains of large length are added to the 3-fold symmetric phenylacetylene nitriles, the volume ratio suggests the formation of a columnar structure, but the local geometry requirements could require the continued formation of the perforated layer structure. Our results for crystal **21** suggest but do not prove that this local geometry requirement is preminent.

A study of long-chain aliphatic carboxylic acid structures shows that in such extreme cases, although the interfacial surface areas are important, the exact volume percentage ranges shown in Figure 4 are no longer maintained.^{122,123} Thus, for long aliphatic chain carboxylic acids, while the overall interface between the hydrophilic acid group and the hydrophobic aliphatic chains are quite flat, presumably due to a minimization of hydrophilic-to-hydrophobic contact, only lamellar structures are found. This result appears to be independent of the aliphatic chain length and hence is independent of the hydrophilic-to-hydrophobic volume ratio. In these crystals, the energy requirement of the perfect interdigitation of the aliphatic chains seems to prevent the formation of columnar or spherical structures.

Crystal Database. The previously described crystal structures suggest within the family of phenylacetylene nitrile compounds with pendant oligo(ethylene oxide) side chains a reasonably sharp evolution of amphiphilic structure types is observed as a function of the hydrophilic-to-hydrophobic volume ratios. We therefore searched the Cambridge Structural Database (CSD) to see if this evolution of structures was to be found in this much larger crystal set. In Figure 7 we illustrate the core unit of our search as well as two illustrative examples of the molecules uncovered. We considered molecules containing only carbon, oxygen, and hydrogen atoms and further required that all sp³ carbon atoms were adjacent to an oxygen atom. None of the thus revealed structures were phenylacetylene-type molecules with pendant oligo(ethylene oxide) side chains. In fact, no pendant side chains were found. Rather the two main

(121) Shetty, A. S.; Zhang, J. S.; Moore, J. S. *J. Am. Chem. Soc.* **1996**, *118*, 1019.

(122) Abrahamsson, S.; Lundén, B. M. *Acta Crystallogr., Sect. B* **1972**, *28*, 2562.

(123) Taga, T.; Miyasaka, T. *Acta Crystallogr., Sect. C* **1987**, *43*, 748.

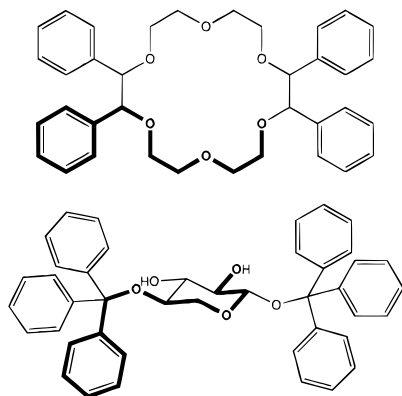


Figure 7. Representative molecules from CSD search. Top: *tranal10*, a functionalized sugar molecule; bottom: *cenpam*, a crown ether. Bold lines represent the CSD search fragment.

Table 3. Correlation between Structure Types and Hydrophobic-to-Hydrophilic Volume Ratios^a

hydrophobic-to-hydrophilic volume ratios (%)	S	C	PL	BI	L	IPL	IC	IS
0–10	–	1	–	–	–	–	–	–
10–20	–	1	–	–	–	–	–	–
20–30	2	8	1	–	–	–	–	–
30–40	–	9	4	2	3	–	–	–
40–50	–	–	–	5	5	–	–	–
50–60	–	–	–	–	1	3	1	–
60–70	–	–	–	–	–	1	–	–
70–80	–	–	–	–	–	–	1	–
80–90	–	–	–	–	–	–	–	1

^a Structural classification is based on closest contacts defined as less than 1.3 times the sum of the van der Waals radii. S: sphere, C: column, PL: perforated layer, BI: bicontinuous, L: layer, IPL: inverse perforated layer, IC: inverse column, IS: inverse sphere.

types found were either crown ether or sugar molecules to which aromatic groups have been attached. Although these molecules therefore contain certain common features with the crystals previously described in this paper, they are sufficiently different to test the extrapolative ability of the overall amphiphilic phase diagram shown in Figure 4. It is therefore gratifying to see that of the 38 structures found all but three were of spherical, columnar, perforated lamellar, lamellar, or bicontinuous types. Of the three exceptions, one structure has overly large voids, suggesting that solvent molecules have not been located, a second by inspection clearly appears to be bicontinuous, and only the last structure fundamentally does not correspond to the previously discussed topological types.

We show these molecules and their corresponding crystal structures in the Supporting Information. The compounds are classified as spherical, columnar, perforated lamellar, lamellar, bicontinuous, inverse perforated lamellar, inverse columnar, and inverse spherical. In the latter three structures, the minor component is hydrophilic, and the major component is hydrophobic. We used the same criterion as described in the previous section to assign volume ratios and structure types. In particular, we considered all aliphatic carbon atoms bonded to oxygen atoms to be hydrophilic. In Table 3, we divide the structures by types and volume ratios. Included in Table 3 are the 13 crystal structures reported in this paper. For the sake of simplicity we report volume ratios for only one set of criteria. We assume that all sp^3 carbon atoms bonded to oxygen atoms are hydrophilic. For structure type assignment we use the method

outlined in the previous section and use the criterion of 1.3 times the sum of the van der Waals radii as a close contact. Again only 10–15% of the structures change their classification in changing this value from 1.3 to 1.15.

As Table 3 shows, there is a clear evolution of structure types as one traverses the possible values of volume ratios. Furthermore, the results of Table 3 are in substantial agreement with the qualitative picture presented in Figure 4. The progression of structures proceeds from spherical to columnar, perforated lamellar, lamellar, bicontinuous, inverse perforated lamellar, inverse columnar, and finally inverse spherical. One distinction between the results in Table 3 and Figure 4 are for the bicontinuous phases. While in Figure 4 the bicontinuous phase is found at lower volume ratios than the lamellar phase, in Table 3 these two phases occupy the same general volume ratio region. This result may be understood if we note that both the bicontinuous and lamellar structure types are self-complementary, that is to say that the regions of space occupied by the hydrophobic and hydrophilic components are topologically similar. Therefore, unlike the perforated layer and inverse perforated layer structures, the bicontinuous structures which flank the lamellar phase in Figure 4 are actually in the same topological family and not two different families. With the broadening of the boundaries, as is found in Table 3, these two groups diffuse into one another, causing the bicontinuous phases to be found at volume ratios such as those of the authentic layer phases.

Taken together these crystal structures show that hydrophilic-to-hydrophobic volume ratios are a significant factor in the final crystal structure adopted. There are, of course, a number of other important variables. For example, as Table 3 shows, there is one columnar structure where the volume ratio is less than 10%. We might have supposed that only spherical structures would have been found at such low ratios. An examination of this structure, which is shown in the Supporting Information, shows that the columns in question are π – π stacks of parallel aromatic rings. Thus, the energetic stability of such stacks outweighs the minimization of hydrophobic-to-hydrophilic contact.

If we are to use volume ratios as an aid in the prediction of desired structural topologies, it therefore appears wisest to consider those fortunate compounds where both surface effects and local geometry predispose the molecules to pack in one unique and obvious manner. It is our belief in such cases that the judicious use of the generic amphiphilic phase diagram and the concomitant restriction to synthetic targets of columnar, lamellar, perforated lamellar, or bicontinuous structure type can be an aid in translating molecular structure to crystal structure.

Acknowledgment. This work was supported by the National Science Foundation (Grant DMR-9812351). We thank Ms. Susan Wilson for assisting in the calculation of volume ratios.

Supporting Information Available: Figures of the molecules from CSD search and their corresponding crystal structures; tables of crystal refinement data, bond distances, bond angles, anisotropic thermal factors for compounds **9–21** and van der Waals radii and bond lengths used in molecular modeling. Experimental and calculated powder diffraction data for the crystalline compounds (PDF). This material is available free of charge via the Internet at <http://pubs.acs.org>.